# Synthetic Analogues of Nickel Superoxide Dismutase: A New Role for Nickel in Biology

Ellen P. Broering, Phan T. Truong, Eric M. Gale, and Todd C. Harrop*

Department of Chemistry and Center for Metalloenzyme Studies, The University of Georgia, 1001 Cedar Street, Athens, Georgia 30602, United States

ABSTRACT: Nickel-containing superoxide dismutases (NiSODs) represent a novel approach to the detoxification of superoxide in biology and thus contribute to the biodiversity of mechanisms for the removal of reactive oxygen species (ROS). While Ni ions play critical roles in anaerobic microbial redox (hydrogenases and CO dehydrogenase/acetyl coenzyme A synthase), they have never been associated with oxygen metabolism. Several SODs have been characterized from numerous sources and are classified by their catalytic metal as Cu/ZnSOD, MnSOD, or FeSOD. Whereas aqueous solutions of Cu(II), Mn(II), and Fe(II) ions are capable of catalyzing the dismutation of superoxide, solutions of Ni(II) are not. Nonetheless, NiSOD catalyzes the reaction at the diffusion-controlled limit ($\sim 10^9$ M^{-1} s^{-1}). To do this, nature has created a Ni coordination unit with the appropriate Ni(III/II) redox potential (~ 0.090 V vs Ag/AgCl). This potential is achieved by a unique

NiSOD   **NiSOD Analogue**

ligand set comprised of residues from the N-terminus of the protein: Cys2 and Cys6 thiolates, the amino terminus and imidazole side chain of His1, and a peptide N-donor from Cys2. Over the past several years, synthetic modeling efforts by several groups have provided insight into understanding the intrinsic properties of this unusual Ni coordination site. Such analogues have revealed information regarding the (i) electrochemical properties that support Ni-based redox, (ii) oxidative protection and/or stability of the coordinated CysS ligands, (iii) probable H^+ sources for H_2O_2 formation, and (iv) nature of the Ni coordination geometry throughout catalysis. This review includes the results and implications of such biomimetic work as it pertains to the structure and function of NiSOD.
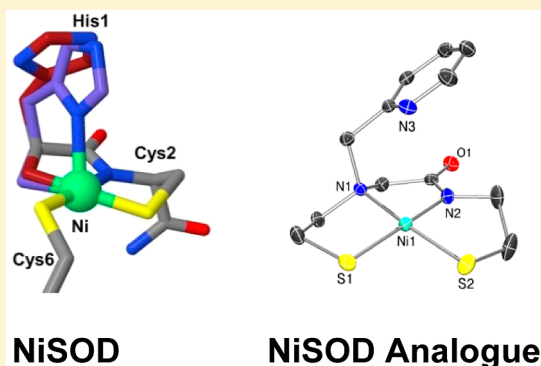
The anionic superoxide radical ($O_2^{\bullet-}$) is an inevitable byproduct of aerobic respiration formed primarily in the mitochondrial matrix upon O_2 reduction along the electron transport chain.[1] If this reactive oxygen species (ROS) is not eliminated, significant damage to surrounding cells will occur, leading to a variety of disease states.[1,2] For example, the formation of ROS such as superoxide has been implicated in diseases such as diabetes,[3] neurological disorders like Parkinson's[4] and Alzheimer's,[5] and the cell death and tissue damage that occur following stroke or heart attack (post-ischemic tissue injury).[6] To combat oxidative stress, all aerobic organisms possess metalloenzyme defense systems known as superoxide dismutases (SODs, EC 1.15.1.1) that catalyze the disproportionation of superoxide to hydrogen peroxide (H_2O_2) and molecular oxygen (O_2) through alternate oxidation and reduction of their respective catalytic metal centers (eqs 1−3).[1,7] Several distinct types of SODs are known, and each is classified by the first-row transition metal utilized to conduct the chemistry.[7a] The more widely studied SODs include the dinuclear Cu/ZnSOD[8] and the mononuclear MnSOD[9] and FeSOD,[9b,c,10] which have been characterized by numerous biochemical, structural, and theoretical techniques. For instance, point mutations in the gene that encodes the mammalian Cu/ZnSOD have been linked with the progression of the neurodegenerative disease Amyotrophic Lateral Sclerosis

(ALS or Lou Gehrig's disease).[11] Several features common to these SODs include (i) a positively charged Lys amino acid channel that guides the anionic substrate toward the active site, (ii) utilization of a metal ion that disproportionates $O_2^{\bullet-}$ even in the free $[M(H_2O)_6]^{n+}$ aquated state, (iii) similarity among the primary coordination spheres of the redox-active metal ion (supported mainly by His-N ligation), and (iv) anion binding affinity at the M^{ox} center supportive of an inner-sphere electron-transfer (eT) mechanism for one of the two SOD half-reactions (eq 1, oxidative half-reaction with respect to substrate).[7b] Recently, a new and distinct class of SOD has been discovered from *Streptomyces* soil bacteria[12] and found in the genome of cyanobacteria[13] that contain Ni at the active site. These SODs show no sequence homology with other SODs, have different and unusual primary coordination spheres, and utilize an active site metal ion not normally associated with oxygen binding or activation. NiSOD thus represents a new role for Ni in a biological context.
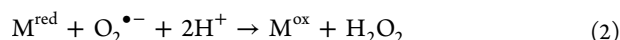
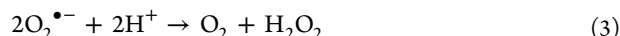$$M^{ox} + O_2^{\bullet-} \rightarrow M^{red} + O_2 \qquad (1)$$

$$M^{red} + O_2^{\bullet -} + 2H^+ \rightarrow M^{ox} + H_2O_2 \qquad (2)$$

Overall

$$2O_2^{\bullet -} + 2H^+ \rightarrow O_2 + H_2O_2 \qquad (3)$$

Structural and Spectroscopic Properties of NiSOD. The structure of NiSOD has been determined by independent groups on two separate *Streptomyces* strains at high resolution (1.30 Å for *Streptomyces coelicolor*[14] and 1.68 Å for *Streptomyces seoulensis*[15]). The separate crystallographic investigations yield nearly identical structures, which is not surprising considering their amino acid sequences are ∼90% homologous. NiSOD is a homohexamer (total molecular mass of 78 kDa) comprised of six interlocked four-helix bundle subunits arranged in the right-handed turn up−down−up−down topology with each subunit housing one solvent inaccessible Ni(III/II) ion (Figure 1). The
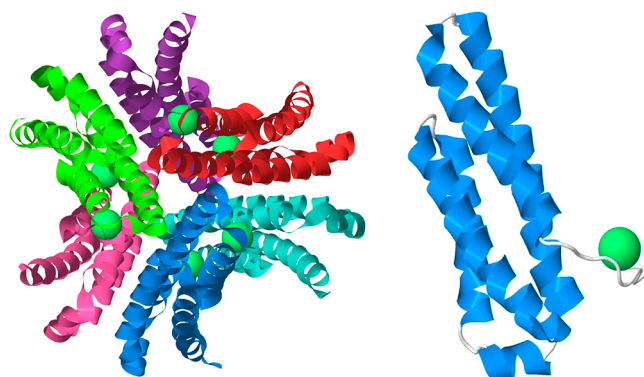

Figure 1. X-ray crystal structure of NiSOD from *S. coelicolor* (1.30 Å resolution, Protein Data Bank entry 1T6U). At the left is the NiSOD biological unit as a hexameric assembly of four-helix bundles. Ni centers are shown as green spheres; subunits are shown in different colors. At the right is the NiSOD subunit with the nickel binding hook. This image was generated with Jmol.

overall protein shape is globular with a hollow inner cavity, which is proposed to be a solvent channel. Depending on the strain, the outer diameter spans 60−72 Å with an interior cavity volume of ∼8800 Å^3 that is 20−23 Å in diameter. The global protein structure and solvent-filled interior are somewhat reminiscent of the ferritin cavity for iron storage. Close examination of the subunits reveals that they are mostly stabilized by hydrophobic intersubunit interactions and salt bridges. The residues primarily responsible for chelating Ni comprise the first nine amino acids from the N-terminus with a recognizable Cys-X-X-X-Cys metal binding motif, i.e., His-Cys-X-X-Pro-Cys-Gly-X-Tyr. It has been proposed that this sequence may be an identifier for NiSOD or a means for detecting NiSOD in future protein isolations from other species. These residues form a hook-like shape and have thus been called the "Ni-hook" region of the protein (Figure 1). Unlike four-helix bundles in other metalloproteins, the Ni-hook protrudes out of the bundle in NiSOD, a novel mode for metal binding among this structural motif. While arguments exist for a positively charged substrate guide by a series of Lys residues that line the active site pocket, calculations reveal no significant positively charged surface residues, which argue against an electrostatic guide. This result is in agreement with the weak ionic strength dependence of the catalytic rate constant (k) for NiSOD.[16]

In both crystal structures of NiSOD, the active site Ni is found in two separate coordination geometries that are dependent on the metal oxidation state (Figure 2). The
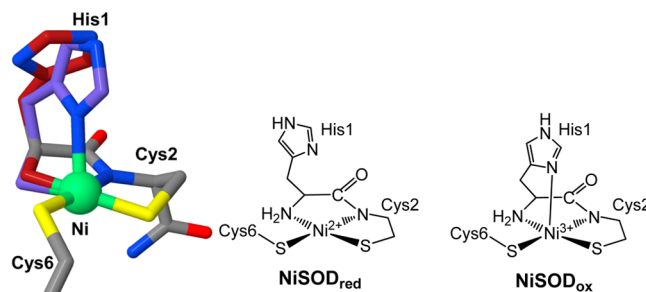

Figure 2. Active site of NiSOD from *S. coelicolor* showing the active site residues involved as ligands to the Ni center (left). The violet depiction of His1 represents the NiSOD$_{ox}$ state, whereas the dark red depiction of His1 represents the NiSOD$_{red}$ state when His1 is noncoordinated. This image was generated with Jmol. At the right is a ChemDraw depiction of the Ni(II) and Ni(III) active site geometries in NiSOD.

mononuclear Ni sites of each subunit appear to operate independently of each other as the shortest Ni−Ni separation is ∼25 Å. Several intersubunit connections, however, could serve as another means of active site communication during catalysis and have been advocated on the basis of mutagenesis studies.[16] As isolated, half of the Ni ions are in the +2 oxidation state and the other half are in the +3 state, highlighting the stability of both states in as-isolated protein. In stark contrast to other known SODs, the reduced form of NiSOD (NiSOD$_{red}$) contains a square-planar Ni(II) ion ligated in an N_2S_2 environment consisting of one deprotonated peptido-N from Cys2, one primary amine-N from the N-terminal His1 residue, and two *cis*-coordinated thiolates from Cys2 and Cys6 (Figure 2). During turnover, superoxide oxidizes the Ni(II)−N_2S_2 site, forming a five-coordinate (5C) square-pyramidal Ni(III)−N_3S_2 species (NiSOD$_{ox}$) via coordination of His1-N$_\delta$ (Figure 2). The Ni−N (1.9−2.1 Å) and Ni−S (2.2−2.3 Å) distances in the basal coordination plane appear to be consistent with other known Ni-metalloenzymes with the same donors as well as small molecule complexes.[17] However, the Ni−HisN distance in NiSOD$_{ox}$ is relatively long (2.3−2.6 Å), which may be explained by the heterogeneity in the crystal structure, i.e., the presence of both Ni(II) and Ni(III) centers. Additionally, a long X-ray exposure time appears to reduce the Ni(III) center in NiSOD$_{ox}$, yielding a NiSOD$_{red}$ structure in which the deligation and C$_\beta$−C$_\gamma$ rotation of the His1 imidazole plane away from the Ni center by ∼3−4 Å can be visualized. On this basis, the structure of NiSOD is very different from its Cu/Zn and Fe, Mn congeners.

NiSOD has unique spectroscopic properties that mainly arise from the high-valent Ni(III) oxidation state.[16,18] The low-spin ($S = ^1/_2$) Ni(III) center in NiSOD$_{ox}$ displays a rhombic EPR spectrum with principal g values of 2.30, 2.24, and 2.01 with a distinct triplet superhyperfine splitting pattern ($A_{zz} = 24.9$ G) in the g_z component consistent with axial N-ligation ($I = 1$) (Figure 3).[14,18a] As isolated, the enzyme contains an equal distribution of Ni(II) and Ni(III) centers that is reflected in the electronic absorption spectrum of the wild-type (WT) holoenzyme.[18b] Because the overall UV−vis spectrum represents a mixture of these oxidation states, researchers have attempted to isolate the pure reduced or oxidized enzyme.
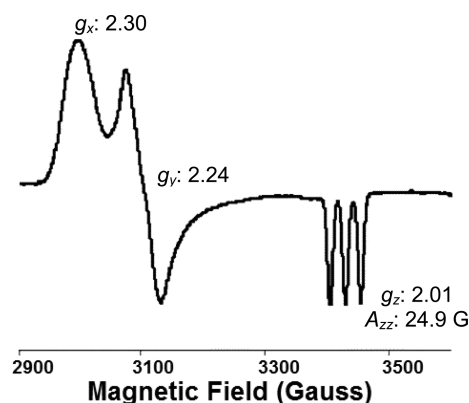
Figure 3. EPR spectrum of as-isolated NiSOD from *S. coelicolor* with selected *g* values. The sample was prepared in 50 mM HEPES buffer (pH 8.0). EPR spectra were collected at 55 K using a microwave frequency of 9.678 GHz, a microwave power of 10 mW, and a modulation amplitude of 5 G. Adapted from ref 14.

The fully reduced enzyme was obtained by chemical reduction with dithionite, which resulted in very weak bands in the UV–vis spectrum. The main features in the visible region in the room-temperature (RT) spectrum are a shoulder at 362 nm (ε = 880 M^{-1} cm^{-1}) and two peaks at 450 nm (ε = 480 M^{-1} cm^{-1}) and 543 nm (ε = 150 M^{-1} cm^{-1}).[18b] These features are hallmarks of square-planar Ni(II)–N_2S_2 coordination complexes,[19] where the λ_{max} peaks have been assigned as ligand-field bands originating from electronic transitions in the d-manifold (d-to-d transitions) of the Ni(II) ion. Subtracting this spectrum from the as-isolated NiSOD spectrum resulted in the UV–vis contributions of NiSOD$_{ox}$. Incidentally, fully oxidized NiSOD could not be obtained even with strong oxidants such as ferricyanide, highlighting the instability of six Ni(III) centers in the protein matrix. The high intensity of the main bands at 372 nm (ε = 6800 M^{-1} cm^{-1}) and 502 nm (ε = 1510 M^{-1} cm^{-1}) are due to sulfur-to-nickel charge-transfer (S-to-Ni CT) bands that are σ and π (i.e., S-pσ to Ni-dσ and S-pπ to Ni-dπ) in origin, respectively.[18b]

The presence of the intense CT band in NiSOD$_{ox}$ allowed for a further probe of the nature of this transition from resonance Raman (rR) experiments.[18b] Excitation into the S–Ni(III) CT at 413.1 nm resulted in three enhanced vibrational modes at 349, 365, and 391 cm^{-1}. From normal coordinate analysis, the 349 and 365 cm^{-1} peaks are more intense than the third and were assigned as ν_{Ni-S} stretching modes of the coordinated sulfur atoms of Cys2 and Cys6. The peak at 391 cm^{-1} was attributed to either a combined Ni–S stretching and S–C_β–C_α–N bending mode of the Cys2 or perhaps to the $\nu_{Ni-N(Cys2)}$ stretching mode. Force constants of the Ni–S bonds were also calculated, resulting in a value of 1.68–1.79 mdyn $Å^{-1}$ for the Ni–S bonds in NiSOD$_{ox}$.[18b,20] This value is characteristic of a high degree of covalency in the Ni–S coordination bond. The covalent nature of the Ni–S bonds in NiSOD has also been supported by further theoretical studies.[18b,20] For comparison, the M–S force constants in NiSOD are on par with those of other classic electron-transfer metalloproteins such as Fe–S clusters (1.2–1.4 mdyn $Å^{-1}$)[21] and blue-copper proteins (~1.9 mdyn $Å^{-1}$).[22] Hence, metallosulfur systems involved in biological electron transfer and/or redox catalysis contain M–S bonds that exhibit a high degree of metal–sulfur covalency.

Analogous to other SODs, NiSOD catalyzes the dismutation reaction near the diffusion-controlled limit with a *k* of 1.3×10^9 M^{-1} s^{-1}.[18a] Furthermore, site-directed mutagenesis studies of the protein have revealed that the axial His1-N ligand is crucial for catalysis.[23] This result was further supported by a rigorous DFT study.[18b] Other mutagenesis studies that reveal the significance of the Cys2 and Cys6 S-ligands[24] and secondary-sphere residues vital for catalysis have also been performed.[16] For example, a combined structural and biochemical study has demonstrated the importance of Tyr9 as a "gatekeeper" residue to allow the $O_2^{\bullet-}$ substrate access to the active site.[16] Similar to those of other SODs,[25] the redox potential of NiSOD is 0.090 V (vs Ag/AgCl, pH 7.4 phosphate buffer),[16] between the corresponding oxidation and reduction potentials for superoxide [$E^{\circ\prime}$ ($O_2/O_2^{\bullet-}$) = −0.360 V, and $E^{\circ\prime}$ ($O_2^{\bullet-}/H_2O_2$) = 0.690 V, respectively (both vs Ag/AgCl, pH 7)].[26] Thus, the novel mixed N/S coordination unit in NiSOD has produced a Ni center that is electrochemically poised to conduct the disproportionation reaction.

NiSOD Questions and Analogue Approach. The atypical coordination sphere and spectroscopy of the redox-active Ni center in NiSOD have generated many questions regarding the structure/function relationship in this enzyme. It is the only SOD that uses a metal whose corresponding aquated species, $[Ni(H_2O)_6]^{2+}$, does not react with $O_2^{\bullet-}$ because its redox potential is >2 V^{27} and well beyond the required potential for SOD chemistry. It is recognized that the unusual set of donor atoms imparts a high degree of covalency to the Ni–L bonds and thus aids in depressing this potential substantially to be within the dismutation window.[9c,18b,28] Unlike the other SODs, which consist primarily of His-N ligation around the catalytic metal, NiSOD contains two CysS residues that are themselves susceptible to ROS.[29] It has been suggested from DFT studies that the inclusion of the deprotonated peptide in combination with the CysS donors, all relatively strong-field ligands, aids in promoting primarily Ni-based redox by destabilizing the Ni(dπ) set of orbitals via strong Ni–ligand–π–antibonding interactions [dπ–pπ repulsions (see Summary and Outlook)].[18b,30] In this regard, CysS ligation is a logical choice because it appears to promote redox-driven reactions at other biological Ni centers and is a prerequisite for redox-active Ni metalloenzymes; NiFe-hydrogenase, the Ni$_p$Ni$_d$ site of the A-cluster, and the NiFe-cubane of the C-cluster of acetyl-CoA synthase/CO dehydrogenase are relevant examples.[17,31,32] Another distinction from other SODs is the low affinity of the Ni center for anions like azide (N_3^-), a common substitute for $O_2^{\bullet-}$, as other SODs bind this anion in their oxidized form, suggestive of an outer-sphere mechanism for NiSOD. Lastly, the identity of potential H^+-donors for the reductive half-reaction (eq 2) to form H_2O_2 is unknown. Several possible donors have been suggested, including a nearby tyrosine residue (Tyr9), the protonated imidazole-N_ε of His1, and Cys2 or Cys6 in the form of a coordinated thiol.[30b,33]

NiSODs are certainly outliers in the SOD family. They contain a different overall protein fold, metal center, ligand environment and geometry, and spectroscopic properties. The $N_{2/3}S_2$ environment is rather unusual for a metal center that involves interaction with and conversion of ROS because the CysS resides are themselves quite susceptible to the formation of S-oxygenates (SO_x) or disulfides.[29] The unusual chemical nature of the N-ligands should also be noted as N-terminal amine coordination has been observed only in the CO sensor CooA,[34] and deprotonated peptido-N ligation is present in only

three other metalloenzymes (nitrile hydratase,[35] the Ni_d site of acetyl-coenzyme A synthase/CO dehydrogenase,[36] and the oxidized P-cluster of nitrogenase[37]).

In summary, the presence of the unique primary coordination sphere in NiSOD has led the bioinorganic community to pose several fundamental questions regarding this enzyme. (i) What intrinsic properties do the coordinated amino acid ligands, which include two CysS residues, a primary amine-N, and a deprotonated peptido-N, impart on the Ni center? (ii) How does such a coordination sphere modulate the redox properties of the Ni center allowing the substrate ($O_2^{\bullet -}$) to preferentially react with Ni to undergo facile one-electron oxidation and reduction and not react with the coordinated CysS residues? (iii) How does nature utilize Ni, typically not considered an O_2 derivative activator/regulator, to react with and disproportionate $O_2^{\bullet -}$; i.e., what is the catalytic mechanism? The fundamental biochemistry that governs the dismutation reaction at the Ni site has initiated the construction of low-molecular weight (MW) complexes (also termed "synthetic models/analogues" or "biomimetics") that reproduce the primary coordination environment observed in the enzyme. This method has been labeled as the synthetic analogue approach,[38] a paradigm in bioinorganic chemistry that has provided valuable information about the structure and mechanism of numerous metalloenzymes. The objective of such an approach is to gain fundamental insight into the structural and electronic properties of the metal active site germane to catalysis through simpler, low-MW constructs. For NiSOD, some of the important criteria for the design and synthesis of suitable models are as follows. (i) First, the ligand frame must contain a mixed nitrogen/sulfur (N/S) donor set to mimic the primary coordination sphere observed in the enzyme. Indeed, the prerequisite for redox-active Ni in biology is coordination of CysS ligands. (ii) Second, and beyond a mere stoichiometric replication of the donor atoms, is the electronic nature of the N/S frame and spatial disposition of the donor atoms. The ligand construct must contain one deprotonatable peptide-N (carboxamide-N is the more general terminology), one primary amine-N, and two *cis*-thiolates situated in a planar N_2S_2 arrangement. An additional neutral N-donor ligand (an imidazole-N is preferable) would be required to replicate the low-spin 4C-to-5C Ni(II/III)SOD redox conversion. (iii) Third, the ligand construct should be amenable to a variety of straightforward modifications much like the environment in the protein matrix of NiSOD. For example, secondary structure, H-bonding, or electrostatic interactions should be considered in construction of the model. This important last requirement will allow for electronic and structural "fine-tuning" of the biomimetic for its desirable function of superoxide dismutation.

Several groups have employed some or all of these criteria by utilizing (i) small peptides or peptide maquettes typically 3−12 amino acids long that mimic the NiSOD primary sequence,[39] (ii) mixed N/S or N/O ligand frames that approximate some aspect of the electronic or structural nature of the NiSOD donors,[40] (iii) electronically accurate N_2S_2 or N_3S_2 frames,[41] (iv) asymmetric N_2S ligands that approximate the Ni active site with an open coordination site where exogenous N-donors bind (NiN_3S),[42] and (v) asymmetric N_2S ligands with NiSOD accurate donors containing an open coordination site where exogenous S-ligands bind to afford NiN_2S_2 species.[43] In this review, we describe these approaches and their relationship to the active site properties and function in NiSOD. We also propose, at the end, a mechanistic possibility and our current understanding of this unusual metalloenzyme based on the collection of synthetic modeling work in combination with the structural, spectroscopic, and theoretical results for the protein.

■ SYNTHETIC ANALOGUES OF NISOD

This novel SOD class has provided the bioinorganic community with a new system for testing the essential features required for SOD's crucial biological function in ROS regulation. To date (2012), several model systems employing short peptides or longer peptide maquettes (3−12 amino acid residues in length) and low-MW (non-maquette) coordination complexes have been constructed. Synthetic endeavors in low-MW analogues have been split between complexes that replicate some aspect of the NiSOD structure or function yet are not entirely parallel to the electronic properties of the His1, Cys2, and Cys6 ligands in the enzyme. These latter systems are designated as approximate models. Other models that replicate the structural disposition and electronic donor type of that found in NiSOD are labeled as accurate models. Research in the maquette area has been especially active as these molecules replicate some aspect of their biological inspiration, taking advantage of secondary and tertiary structural features offered by the biological peptide scaffold. While the construction of low-MW models that accurately reproduce the primary coordination sphere of NiSOD is not as widespread, synthetic endeavors aimed at these model systems are slowly becoming more prevalent. The knowledge gained from both approaches and the structural, electronic, and mechanistic relevance to NiSOD are presented below.

NiSOD Peptide Analogues. *Synthetic Models Based on Peptide Maquettes.* The first NiSOD maquette model was synthesized by Shearer and co-workers, which was designated $[Ni(SOD^{M1})]$ [**1**, where SOD^{M1} is HCDLPCGVYDPA (Figure 4)].[39a] Several derivatives of **1** were also constructed to electronically modify the His1 ligand, namely, $[Ni(SOD^{M1}$-Im-X)]$ where X = Me (1^{MeIm}), 2,4-dinitrophenyl (1^{DNP}), and tosyl

[Ni(SOD^{M1}-Im-H)] (**1**)   [Ni(SOD^{M1}-Im-Me)] (**1^{MeIm}**)

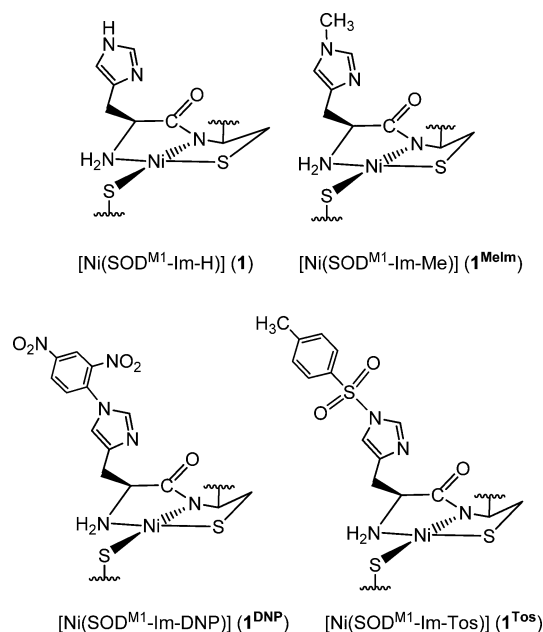[Ni(SOD^{M1}-Im-DNP)] (**1^{DNP}**)   [Ni(SOD^{M1}-Im-Tos)] (**1^{Tos}**)

Figure 4. Structures of the NiSOD maquette models based on $[Ni(SOD^{M1})]$ [SOD^{M1} = H′CDLPCGVYDPA, where H′ = H (**1**), Me (**1^{MeIm}**), 2,4-dinitrophenyl (**1^{DNP}**), and tosyl (**1^{Tos}**)].

Table 1. Spectroscopic, Structural, Electrochemical, and SOD Activity Kinetic Data for NiSOD and NiSOD Maquette Models

complex	λ_{max} (nm) [ε (M^{-1} cm^{-1})]	$E_{1/2}$ (V)[a]	Ni−N, Ni−S (Å)[b]	k (M^{-1} s^{-1})	refs
NiSOD$_{red}$ (S. coelicolor)	450 (480), 543 (150)[c]	0.090[d]	1.89, 2.18	7×10^8	14, 16, 18b
NiSOD$_{red}$ (S. seoulensis)	N/A	N/A	2.01, 2.21	1.3×10^9	15
[Ni(SOD^{M1}-Im-H)] (**1**)	458 (510), 552 (240)[e]	0.434[e]	1.93, 2.180	$4(3) \times 10^7$	39a
[Ni(SOD^{M1}-Im-Me)] (**1^{MeIm}**)	461 (360), 554 (160 sh)[e]	0.282[e]	1.91, 2.182	$6(1) \times 10^6$	39c
[Ni(SOD^{M1}-Im-DNP)] (**1^{DNP}**)	464 (410 sh), 552 (150 sh)[e]	0.470[e]	1.89, 2.179	$3(2) \times 10^8$	39c
[Ni(SOD^{M1}-Im-Tos)] (**1^{Tos}**)	460 (405 sh), 552 (180 sh)[e]	0.598[e]	1.87, 2.174	$6(2) \times 10^8$	39c
[Ni(SOD^{M2})] (**2**)	457 (345), 548 (130 sh)[e]	0.520[e]	1.875, 2.176	$1(1) \times 10^{-6}$ M (IC$_{50}$)[f]	39b
[Ni(mSOD)] (**3**)	454 (432)[g]	N/A	N/A	830 units/μmol[h]	39d, 39e

[a]Data represent the $E_{1/2}$ value for the Ni(III/II) redox couple normalized to the Ag/AgCl reference electrode [E vs NHE = E vs Ag/AgCl(saturated KCl) + 0.199 V] based on information found in ref 46. [b]Ni−S and Ni−N bond distances represent the averages of the two distinct sets of CysS-donors and N-donors from the X-ray crystal structure of NiSOD; metric parameters for the maquette systems were obtained by EXAFS, which cannot distinguish between these sets of atoms. [c]Tris buffer (pH 8.5). [d]Potassium phosphate buffer (pH 7.5). [e]NEM buffer (pH 7.4). [f]Only IC$_{50}$ value measured for **2** where IC$_{50}$ is the concentration of SOD mimic required to effect a 50% reduction in the rate of formazan formation; the IC$_{50}$ for Cu/ZnSOD is 4×10^{-8} M. [g]Nonbuffered, deionized H$_2$O/NaOH mixture measured at pH 7.8. [h]The 1:1 Ni/peptide activity provided (see the text). The activity is defined as the half-limited reduction of NBT by superoxide where 1 unit = 2(Abs$_{NBT-control}$ − Abs$_{NBT-maquette}$)/Abs$_{NBT-control}$; the activity of NiSOD (S. coelicolor) is ~45000 units/μmol per subunit (see ref 39d).

(**1^{Tos}**) (Figure 4).[39c] This base maquette is comprised of the first 12 residues from the S. coelicolor primary sequence and was shown to coordinate Ni(II) in a 1:1 Ni:peptide ratio under slightly basic conditions. Neutral to slightly acidic conditions did not afford the Ni-coordinated maquettes likely because of protonation of the CysS and peptide-N ligands at these pH values. Additionally, the Ni systems are unstable to air over the course of hours and yield intractable high-MW polymeric species upon exposure. Yields for **1** and **1^{MeIm}** were stoichiometric; however, yields of **1^{DNP}** and **1^{Tos}** were low (14−21%) because of the sensitivity of the tosyl and 2,4-dinitrophenyl functional groups to workup conditions. All of the Ni peptides were characterized by UV−vis, X-ray absorption spectroscopy (XAS), and electrochemistry (results listed in Table 1). For example, **1** and its derivatives afforded light beige-pink-colored solutions originating from the low-intensity ligand-field band at λ_{avg} = 461 nm (ε_{avg} = 420 M^{-1} cm^{-1}) with a shoulder at λ_{avg} = 553 nm (ε_{avg} = 180 M^{-1} cm^{-1}) in pH 7.4 NEM buffer. These electronic transitions are typical of Ni(II) housed in a planar N$_2$S$_2$ coordination sphere.[17,20] XAS further supported the UV−vis data with metric parameters (Ni−N$_{avg}$, 1.90 Å; Ni−S$_{avg}$, 2.179 Å) and edge transitions consistent with a square-planar Ni(II)−N$_2$S$_2$ metal site in all maquettes.[44] The electrochemistry revealed quasi-reversible $E_{1/2}$ values in the cyclic voltammograms (CVs) with the Ni(III/II) couple ranging from 0.280 to 0.600 V (vs Ag/AgCl, pH 7.4 NEM buffer), which trend with the electron-withdrawing (for **1^{DNP}**, $E_{1/2}$ = 0.470 V; for **1^{Tos}**, $E_{1/2}$ = 0.598 V) and electron-donating (for **1^{MeIm}**, $E_{1/2}$ = 0.282 V) nature of the groups attached to the His1-N$_\varepsilon$ imidazole atom (Table 1). All values are within the superoxide disproportionation window, suggesting that these NiSOD maquette models can perform SOD redox chemistry (vide infra). Collectively, the structural and spectroscopic features of maquettes based on **1** are nearly identical and resemble those obtained for NiSOD$_{red}$.

Despite the structural and electronic similarity of the maquettes to NiSOD$_{red}$, accessing Ni(III) was problematic. Achieving this oxidation state (at least transiently) is a requirement to realize functionality in these systems. Indeed, the isolation and characterization of Ni(III) complexes with thiolate ligands is difficult and rare; only one such Ni(III)−thiolate complex has ever been crystallized.[45] Initial attempts to chemically oxidize **1** resulted in decomposition and formation of high-MW polymers. However, utilizing a mild oxidant (I$_2$)

afforded Ni(III) maquettes that could be trapped in situ at low temperatures. The resulting X-band EPR spectra of all Ni(III)-bound peptides are similar [g_{avg} values for g_x (2.34), g_y (2.26), and g_z (2.01) at 77 K] and resemble the rhombic $S = \frac{1}{2}$ EPR spectrum of as-isolated NiSOD (see Figure 3).[14] The superhyperfine coupling in the g_z component (A_{zz}) is also observed in all Ni(III)-bound peptides, which ranges from 18.3 to 26.4 G compared to the A_{zz} value of 24.9 G for NiSOD. Interestingly, the A_{zz} values for **1^{Tos}** and **1^{DNP}** are the closest to that of the enzyme. This value is reflective of the strength of the interaction between the unpaired spin on Ni(III) and the His1 N$_\delta$ ligand, and the relatively long Ni(III)−NIm bond distance in NiSOD$_{ox}$ defines the extent of this coupling in the enzyme. Thus, the Ni maquettes with the electron-withdrawing groups on N$_\varepsilon$ (i.e., the weaker Lewis base) better resemble A_{zz} in NiSOD$_{ox}$ because they contained the longer Ni−NIm bond. Moreover, this electronic modification should correlate with superoxide reaction kinetics. Indeed, **1** and its derivatives are able to catalytically disproportionate superoxide as monitored by stopped-flow kinetics [$k \sim 10^6$–10^8 M^{-1} s^{-1} (Table 1)]. As expected from EPR, complexes **1^{DNP}** and **1^{Tos}** are the most active NiSOD mimetics with k values of $3(2) \times 10^8$ M^{-1} s^{-1} for **1^{DNP}** and $6(2) \times 10^8$ M^{-1} s^{-1} for **1^{Tos}**. These k values are only 1 order of magnitude lower than the diffusion-controlled rate observed for all SODs ($k \sim 10^9$ M^{-1} s^{-1}). Accordingly, the nature of the long axial Ni(III)−NIm bond in NiSOD$_{ox}$ is modeled nicely with the SOD^{M1} maquettes with electronic modifications on the His1 residue.

In a second-generation system, Shearer reported the synthesis and properties of the Ni maquette complex with the heptapeptide SOD^{M2}, namely [Ni(SOD^{M2})] (**2**, where SOD^{M2} = HCDLPCG, a Ni coordination sphere similar to that depicted for **1** in Figure 4).[39b] Analogous to SOD^{M1}, SOD^{M2} and its derivatives coordinated Ni(II) in a 1:1 ratio under slightly basic conditions affording light beige-pink solutions of **2** with similar UV−vis profiles (Table 1). Complex **2** has an appropriate redox potential to act as an SOD [$E_{1/2}$ = 0.520 V vs Ag/AgCl, pH 7.4 NEM (see footnote [a] of Table 1 for conversion to NHE)], contains a Ni(II) center in an N$_2$S$_2$ environment (XAS), does not bind anions such as N$_3^-$, and catalytically disproportionates superoxide. Thus, the removal of the last five residues outside of the Ni-hook of native NiSOD does not compromise the Ni affinity or electronic structure with the smaller peptide in **2**. The CV displays quasi-reversible

behavior with an $E_{ox} - E_{red}$ peak-to-peak separation (ΔE_p) of 0.240 V, which is suggestive of substantial structural rearrangement taking place about the Ni center during redox. The Ni(III)-bound peptides cannot be obtained or isolated in pure form upon chemical oxidation or bulk electrolysis, suggesting, as with **1**, the relative instability of Ni(III) in this environment. However, the Ni(III)-bound peptide was obtained in situ following substoichiometric addition of KO_2 to afford a rhombic EPR spectrum similar to that of NiSOD$_{ox}$.[39b] Activities were measured using a modified xanthine/xanthine oxidase assay and afforded an IC_{50} value (where IC_{50} is the concentration of SOD mimic to effect a 50% reduction in the rate of formazan formation) of 1×10^{-6} M for **2**, 2 orders of magnitude higher than the IC_{50} value of Cu/ZnSOD (4×10^{-8} M). Replacing His1 in **2** with Ala (**2**[Ala]) completely shut off activity, comparable to the H1A mutation in NiSOD.[23] Additional insight from DFT and eT rate calculations at overpotential confirmed that the Ni center in **2** remains 5C when cycling through the Ni(III/II) states. Taken together, maquettes **1** and **2** afford excellent structural and functional models of NiSOD, advocating for a 5C Ni center and outer-sphere eT as probable mechanistic features of this enzyme.

At approximately the same time, the groups of Weston and Buntkowsky reported an extensive study on the properties of a Ni(II) nonapeptide maquette that they label as [Ni(mSOD)] (**3**, where mSOD = HCDLPCGVY) (see Figure 4 for the analogous Ni coordination structure).[39d−g] Similar to the aforementioned NiSOD maquette studies of **1** and **2**, Ni coordinated to mSOD in a mostly 1:1 Ni:peptide ratio in **3** (other ratios were observed on the basis of ESI-MS and UV−vis titrations), affording pink-colored solutions.[39d,e] Although XAS was not performed to define the Ni coordination sphere in this model, solution NMR, UV−vis, and DFT studies were indicative of an N_2S_2 square-planar environment about the Ni(II) ion. The theoretically estimated Ni−N and Ni−S distances are on par with those experimentally observed in maquettes **1** and **2**, suggesting similar Ni coordination environments (Table 1). In contrast to **1** and **2**, an enhanced stability to ambient lab conditions was noted for **3**. The Ni(III) version of this maquette was not isolated; however, DFT computations predict that the ground state of Ni(III)-mSOD is a triplet and thus high-spin. This result is opposite to what is found with **1**, **2**, and the native enzyme. The $S = 1$ state for Ni(III)-mSOD is supposedly due to the fifth axial ligand arising from the neutral carbonyl-O of the Leu4-Pro5 peptide backbone, rather than axial binding of His1 as seen in **1**, **2**, and NiSOD$_{ox}$. This dissimilar coordination environment is due to a conformational difference with respect to Pro5: in NiSOD, Pro5 is in a *cis* conformation, whereas in **3**, Pro5 is orientated in a *trans* configuration because of H-bonding interactions of the peptide. It was suggested that the Pro5 *trans* arrangement prevents His1-N$_\delta$ from binding, and it was also proposed to prevent the binding of superoxide opposite to His1. The activity of maquette **3** is thus considerably lower than that of native NiSOD (vide infra). As such, a new maquette was constructed to enforce the *cis* conformation observed in the enzyme.[39f] However, this maquette did not affect the reactivity, suggesting that this structural perturbation is not responsible for the low activity of these maquettes.

Reactivity studies were conducted with **3** in the presence of KO_2 using the nitroblue tetrazolium (NBT) assay, and it was shown to be stable for 60−90 s.[39d] In attempts to account for both 1:1 and 2:1 stoichiometries for the Ni−peptide complexes

in solution, the xanthine/xanthine oxidase assay was run to establish lower and upper limits of $O_2^{\bullet-}$ activity. The 1:1 complex produced an activity value of 830 units μmol^{-1} [activity defined as the half-limited reduction of NBT by superoxide where 1 unit = $2(Abs_{NBT-control} - Abs_{NBT-maquette})/Abs_{NBT-control}$]; the 2:1 ratio resulted in an activity of 1250 units μmol^{-1}, demonstrating that the nine-residue peptide can serve as a functional NiSOD mimic. Activity studies were repeated with a mutated peptide for which His1 was replaced with Ala to yield a negligible decrease in activity, disputing the essentiality of His1 for catalytic activity. It was proposed instead that Pro5 is responsible for tuning the oxidation state of the biomimetic, as the *trans*-Pro5 residue prevents an axial histidine nitrogen atom from binding to Ni(III) in this maquette.

Further reactivity of **3** was performed using cyanide anion (CN$^-$) as a substrate analogue.[39e] Complexes **1** and **2** show no evidence of binding anions such as azide, and CN$^-$ strips the Ni(II) center from the peptide, all pointing toward an outer-sphere mechanism for NiSOD (vide supra). Upon addition of 1 equiv of CN$^-$ to **3**, the pink solution turned yellow, consistent with a change in the Ni coordination environment. Indeed, MS experiments confirmed the presence of the mono-CN$^-$ adduct of the Ni maquette, [Ni(mSOD)(CN)] (**4**). The UV−vis spectrum of **4** in a pH 7.8 H_2O/NaOH nonbuffered medium revealed mostly UV transitions ($\lambda = 252$ nm, $\varepsilon = 12000$ M^{-1} cm^{-1}, and $\lambda_{sh} = 282$ nm) and one visible band at 410 nm ($\varepsilon = 180$ M^{-1} cm^{-1}). The resulting electronic transitions of **4** all blue-shift from the parent Ni(II) square-planar species **3** (see Table 1). The formation of **4** was further confirmed by ^{13}C and ^{15}N NMR and FTIR spectroscopy, which revealed one strong and single ν_{CN} peak at 2108 cm^{-1} (KBr).

Collectively, the properties and reaction chemistry of peptide maquettes **1**−**3** provide a somewhat unifying picture of Ni in the SOD coordination sphere. The Ni(II)−N_2S_2 square-planar coordination environment is maintained throughout and affords similar metric parameters and electronic absorption profiles (see Table 1). Maquettes **1** and **2** break down and form intractable polymeric species upon being exposed to air within hours, whereas maquette **3** was stable for days at RT and weeks at 4 °C. The defining feature of the oxidative stability is unknown at present. All of the Ni maquettes disproportionate $O_2^{\bullet-}$ at rates higher than the spontaneous rate but significantly lower than the rate of NiSOD. Ni(III) forms of the maquettes are difficult to obtain; however, in situ EPR isolation of Ni(III) maquettes **1** and **2** has been successful, and in one case, a Ni(III) species has been confirmed by XAS (**1**[MeIm]). One defining feature of maquette **3** is the stoichiometric binding of CN$^-$, a property that supports inner-sphere coordination and eT to $O_2^{\bullet-}$ in NiSOD. Furthermore, replacement of His with Ala does not significantly change the rate in **3**. This result is quite in contrast to the same modification in the enzyme and in maquette **2**. Perhaps the carbonyl-O ligand from Pro5 in **3** supports the SOD reaction, albeit through a mechanism different from that in NiSOD. It is difficult to delineate the variances between the system of Shearer and the system of Weston and Buntkowsky. Perhaps the noted differences lie in the relative instability of some of the maquettes. For example, the nonapeptide Ni maquette **3** is shown to exist in equilibrium with 2:1 and 1:1 Ni−peptide species in solution. This observation alone warrants the need for more definitive structural information on **3** or more discrete and crystallizable small molecule analogues. The work on maquette **3** is also controversial as a separate publication from the same group

states that only a 1:1 species exists.[39e,g] Additionally, the electronic similarity of $O_2^{\bullet-}$ and CN^- is a bit of a stretch, and one would expect Ni (or any transition metal) to bind the strong-field CN^- ligand. The CN^- binding results are also contradictory to those of the anion binding studies performed on the enzyme and in the maquettes of Shearer. Their experiments reveal that CN^-, rather than binding, strips the Ni from the model to form $[Ni(CN)_4]^{2-}$, which may be explained by the use of excess CN^-.[39b] In contrast, Buntkowsky proposed that by limiting the stoichiometry to 1 equiv, CN^- can bind to the metal center without disrupting the coordination sphere and that this binding capability should translate to the native enzyme. As of 2012, binding of an anion to the Ni center in NiSOD (ox or red) has yet to be established. Taken together, it appears that the minimal requirement to achieve functionality in these maquettes is the first seven amino acid residues of the Ni-hook as this length appears to bind Ni with high affinity and provides suitable aqueous stability. Additionally, special attention must be given to the positioning of the His1-Im in these maquettes for proper binding to the Ni center so that Ni(III/II) redox cycling is facile and turnover is fast.

NiSOD Low-MW Analogues. *NiSOD Approximate Models.* The work on approximate models of NiSOD has utilized a variety of different ligand platforms that incorporate some but not all features of the biological coordination unit. The first low-MW NiSOD model complex that demonstrated SOD activity was synthesized by Darensbourg and co-workers in 2009.[42a] They employed the ligand 1-(2-mercapto-2-methylpropyl)methyl-1,4-diazacycloheptane (mmp-dachH, where H is a dissociable proton) as an amine-thiol N_2S chelate for Ni (Figure 5). Reaction of the deprotonated ligand with
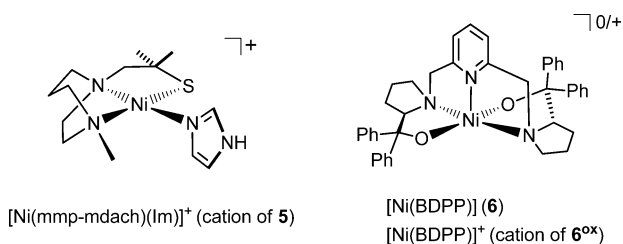

Figure 5. Structures of the NiSOD approximate model complexes [Ni(mmp-mdach)(Im)]Cl (**5**, left) and [Ni(BDPP)] (**6**, right)/[Ni(BDPP)]PF$_6$ (**6^{ox}**, right). Ph is phenyl or C_6H_5 for the structures of **6** and **6^{ox}**, respectively.

Ni(II) salts resulted in a dimeric Ni(II) complex with bridging alkyl thiolates (S,S-bridged or μ-thiolato bridge) that approximated the N_2S_2 coordination sphere of NiSOD$_{red}$. Because the active sites of NiSOD function as discrete monomeric species, attempts were made to cleave the μ-thiolato core with biologically relevant ligands. Although this reaction appears feasible, it has not been widely adopted as a successful approach to accessing monomeric Ni–thiolato complexes. Bridge splitting of the dimer with imidazole (Im) afforded the monomeric Ni(II) complex [Ni(mmp-mdach)(Im)]Cl (**5**) (Figure 5). The geometry about the Ni(II) center in **5** is square-planar arising from the N_2S ligand and the monodentate Im to afford an N_3S chromophore. The Ni–S distance (2.149 Å) is typical for planar Ni–thiolate complexes and similar to that of NiSOD, but the Ni–N_{Im} distance is short (1.888 Å) and unlike the enzyme value (~2.3–2.5 Å) because of its location in the equatorial plane. This complex was the first

structurally characterized Ni(II) species containing both thiolate and imidazole donors, both of which are key ligands in NiSOD albeit in different positions in the coordination sphere (see Figure 5). This orange complex displayed one d–d band in the visible region at 467 nm (ε = 500 M^{-1} cm^{-1}), which is different from Ni(II)–N_2S_2 complexes and NiSOD$_{red}$. The CV of **5** exhibited an irreversible oxidation wave (E_{ox}) at 0.43 V in DMF (vs Ag/AgCl), which has been attributed to thiolate oxidation of the mmp-mdach ligand. This property would suggest that **5** would not be a functional SOD mimic. However, an aqueous solution of **5** (61 μM) provided protection against 100 equiv of $O_2^{\bullet-}$ to NBT (61 μM), preventing formazan formation by ~40% in pH 7.4 phosphate buffer. Furthermore, this complex is stable to O_2 and affords S-oxygenated species when reacted with H_2O_2. Thus, this model implies that the mixed N/S-donors of NiSOD provide O_2-stability to the coordination unit. The exact role of the Ni center in the SOD chemistry was not defined; however, **5** was the first example of a NiSOD functional model.

The first 5C analogue of NiSOD was described in late 2011 by Kuo and co-workers utilizing an N_3O_2 chelate.[40c] The pentadentate ligand, 2,6-bis{[(S)-2-(diphenylhydroxymethyl)-1-pyrrolidinyl]methyl}pyridine (H$_2$BDPP, where H represents dissociable protons), employed nonbiological donor atoms that included one pyridine-N, two tertiary pyrrolidine-N atoms, and two alcohol-O donors. Because of the steric restrictions imposed by the ligand frame, the pyridine-N was forced into an axial position upon coordination to Ni regardless of the oxidation state, a clever design strategy to impose a 5C geometry. The resulting Ni(II) complex [Ni(BDPP)] (**6**) contained a Ni(II) center in a distorted square-pyramidal N_3O_2 environment that structurally replicated the 5C geometry of NiSOD$_{ox}$ (Figure 5). The X-ray structure of **6** revealed a Ni–N_{py} distance of 1.969 Å with two longer Ni–N_{avg} distances (2.149 Å) from the pyrrolidines and two short Ni–O_{avg} bonds (1.930 Å) from the tertiary O-donors in a *trans* configuration (Figure 5). The bond distances in **6** advocate for a diamagnetic low-spin (S = 0) 5C Ni(II) center, although no other evidence was presented to support this electronic configuration. The pale green complex exhibited a quasi-reversible CV with an $E_{1/2}$ of 0.308 V (vs Ag/AgCl in CH_2Cl_2), suggesting that the BDPP^{2-} ligand could support Ni(III) with minimal structural rearrangement. Indeed, chemical oxidation of **6** cleanly yielded the Ni(III) complex [Ni(BDPP)](PF$_6$) (**6^{ox}**) that was structurally characterized by X-ray crystallography. As expected, the Ni–L distances in **6^{ox}** contracted (~0.1 Å for equatorial ligands; ~0.02 Å for the axial Ni–N_{py} distance) from the parent Ni(II) complex **6** because of decreased Ni–ligand electron repulsion (Ni–N_{py}, 1.947 Å; Ni–$N_{pyrrolidine}$, 2.045 Å; Ni–O, 1.844 Å). In contrast to that of NiSOD$_{ox}$, the X-band EPR spectrum of **6^{ox}** afforded an axial signal because of the high degree of symmetry and electronic equivalency of the *trans*-N_2O_2 donors in the basal plane ($g_x = g_y$ = 2.18 and g_z = 2.04 in CH_2Cl_2 at 77 K) (see Figure 3 for NiSOD$_{ox}$). The hyperfine coupling in the g_z component in **6^{ox}** (A_{zz} = 25.0 G), however, is identical to the coupling in the enzyme. Both of these hyperfine patterns are due to the axial N-ligand. In fact, DFT studies confirm that the majority of the spin density in **6^{ox}** resides in an MO with significant Ni d_{z^2} character much like that of NiSOD$_{ox}$.[18b] Taken together, the data suggest that **6** or **6^{ox}** should be capable of $O_2^{\bullet-}$ disproportionation. Indeed, **6^{ox}** was shown to react with excess KO$_2$ in MeCN to produce O_2 and Ni(II) complex **6** in stoichiometric yields. Interestingly, Ni(II) complex **6** did not

react with KO_2 to produce H_2O_2. Despite the presence of the RO^- ligands, the spin-state of the Ni center appears to remain low-spin in both Ni oxidation states. This spin-state appears to be a requisite for catalysis as high-spin Ni(III/II) has never been found in enzyme preparations, nor would it be of the appropriate redox potential. Additionally, this model appears to be at odds with data from Cys-to-Ser mutations in the enzyme. This mutation resulted in high-spin Ni(II) centers that could not access the high-valent Ni(III) state.[24] Ultimately, this mutation afforded inactive NiSOD. It appears that careful construction of the ligand frame to house 5C and low-spin Ni(II) could be an additional requirement for a functional NiSOD model.

NiSOD Accurate Models. The first low-MW analogue that accurately reproduced the NiSOD primary coordination sphere was the square-planar Ni(II)−N_2S_2 complex, (Me$_4$N)[Ni-(BEAAM)] [7 (Figure 6)].[41a] This orange-colored complex

[Ni(BEAAM)]⁻ (anion of 7)   [Ni(HL2)]⁻ (anion of 8)
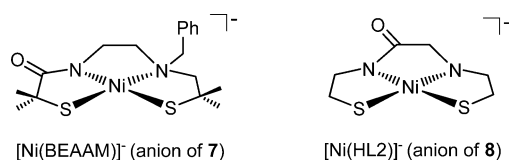
Figure 6. Structures of NiSOD model complexes (Me$_4$N)[Ni-(BEAAM)] (7, left) and K[Ni(HL2)] (8, right). Ph is phenyl or C_6H_5 for the structure of 7.

was structurally characterized by X-ray crystallography and consists of an $N_{amine}N_{carboxamide}S_2$ chromophore with asymmetric Ni−N bonds because of the electronic differences in the N-donors. The spectroscopic and structural properties are summarized in Table 2. For example, the Ni−N_{amine} bond is notably longer (1.989 Å) than the Ni−$N_{carboxamide}$ bond (1.858 Å). The high resolution of small molecule crystallography has provided the electronic discrepancy in these two Ni−N bonds that is absent in the EXAFS data of maquette systems 1 and 2. The variance in the Ni−N bond lengths is due to the good σ-donating ability of the carboxamido-N, which provides for more covalency in this bond. These effects are also manifested in the Ni−S bond which it is *trans* to. The Ni−S bond *trans* to the carboxamido-N is significantly elongated (2.177 Å) with respect to the Ni−S bond *trans* to the amine (2.137 Å). A similar difference is observed in the Ni−S distances of NiSOD$_{red}$ (S.

coelicolor).[14] Analogous to those of the maquette systems and the enzyme, a double-humped UV−vis spectrum is observed with ligand-field transitions at 461 nm ($\varepsilon = 290$ M^{-1} cm^{-1}) and 556 nm ($\varepsilon = 70$ M^{-1} cm^{-1}) in MeCN underscoring the electronic equivalence of this model and NiSOD$_{red}$. The quasi-reversible Ni(III/II) couple observed for 7 at 0.120 V (vs Ag/AgCl in MeCN) is also within the potential window for SOD chemistry, but the complex does not react with $O_2^{•-}$. Additionally, bulk oxidation studies at low temperature resulted in the formation of a short-lived purple/blue species that is nonisolable, and no other spectroscopic evidence was provided for this oxidized species. The axial N-ligand, which is notably absent from this complex, may be necessary for the stabilization of Ni(III) in these models and in NiSOD.

In a follow-up to this communication, Shearer and Hegg reported the NiSOD model, K[Ni(HL2)] [8 (Figure 6)], with a similar N_2S_2 ligand frame as in 7 but with the absence of the *gem*-dimethyl groups on the carbon atoms α to sulfur.[41b] The metric parameters and electronic absorption spectrum are very similar between the two complexes (Table 2), suggesting analogous structural and electronic properties. One noted difference, however, is in the CV data, which displayed an irreversible oxidation for 8 at 0.065 V (vs Ag/AgCl in DMF) indicative of ligand-based redox. Additionally, attempts to chemically oxidize 8 at low temperatures resulted in an EPR-inactive species that supports S-oxidation to disulfide. The difference in CV data between otherwise structurally (and presumably electronically) equivalent Ni(II) centers was puzzling. The DFT-generated redox-active MOs in 7 and 8 revealed a significant change in the amounts of S-pπ and Ni-dπ character in these complexes. For example, the Ni-character in 8 (32% Ni-dπ, 68% S-pπ) is much lower (and S-character higher) than in 7 (56% Ni-dπ, 32% S-pπ). While the ligand frames are similar, it appears that the methyl substituents on the ligand in 7 clearly aid in stabilizing and supporting Ni-based redox and access to the Ni(III) oxidation state. Even though both complexes do not react with superoxide, the clear differences in the CVs reveal key factors for obtaining at least Ni(III) in this asymmetric N/S coordination environment by providing steric bulk and enhanced Lewis basicity at the S-donor. Taken together, the results for complexes 7 and 8 propose that well-defined and controlled modifications at or near the S-ligands in Ni-N_2S_2 coordination units can

Table 2. Spectroscopic, Structural, and Electrochemical Data of NiSOD Low-MW Synthetic Analogues

complex	λ_{max} (nm) [ε (M^{-1} cm^{-1})]	E_{ox} (V)[a]	Ni−N$_{peptide}$, Ni−N$_{amine}$ (Å)	Ni−S$_{trans\text{-}peptide}$, Ni−S$_{trans\text{-}amine}$ (Å)	refs
NiSOD$_{red}$ (S. coelicolor)	450 (480), 543 (150)[b]	0.090[c]	1.91, 1.87	2.19, 2.16	14, 16, 18b
NiSOD$_{red}$ (S. seoulensis)	N/A	N/A	1.94, 2.07	2.18, 2.24	15
(Me$_4$N)[Ni(BEAAM)] (7)	461 (290), 556 (70)[d]	0.120[d]	1.858, 1.989	2.177, 2.137	41a
K[Ni(HL2)] (8)	449 (340), 570 (70 sh)[e]	0.065[f]	1.862, 1.937	2.1711, 2.1671	41b
(Et$_4$N)[Ni(nmp)(SC$_6$H$_4$-p-Cl)] (10)	450 (5450)[d]	0.236[d]	1.8638, 1.9470	2.2139, 2.1492	43a
(Et$_4$N)[Ni(nmp)(S^{t}Bu)] (11)	464 (4540)[d]	0.075[d]	1.882, 1.9635	2.1938, 2.1629	43a
(Et$_4$N)[Ni(nmp)(S-o-babt)] (12)	450 (3500)[d]	0.276[d]	1.877, 1.947	2.1939, 2.1518	43b
(Et$_4$N)[Ni(nmp)(S-meb)] (13)	449 (3900)[d]	0.214[d]	1.863, 1.944	2.172, 2.156	43b
K[Ni(GC-OMe)(SC$_6$H$_4$-p-Cl)] (15)	481 (390), 560 (230)[f]	0.220[f]	1.83, 1.99[g]	2.16 (avg.)[g]	43c
K[Ni(GC-OMe)(SNAc)] (17)	463 (350), 545 (160)[f]	0.310[f]	1.83, 1.99[g]	2.17 (avg.)[g]	43c
K[Ni(N$_3$S$_2$)] (19)	449 (320), 570 (90)[e]	−0.125[f]	1.8575, 1.954	2.1805, 2.1739	41c

[a]Data represent the E_{ox} value normalized to the Ag/AgCl reference electrode [E vs NHE = E vs Ag/AgCl(saturated KCl) + 0.199 V] based on information found in ref 46; the quasi-reversible $E_{1/2}$ is reported for 7, and a reversible $E_{1/2}$ is reported for NiSOD, which represent the Ni(III/II) redox couple. [b]Tris buffer (pH 8.5). [c]Potassium phosphate buffer (pH 7.5). [d]MeCN. [e]MeOH. [f]DMF. [g]Metric parameters from EXAFS. The reported Ni−S bond distance represents the average from two separate S scattering atoms.

significantly alter the nature of the frontier MOs that ultimately dictate redox behavior in these systems and presumably in the enzyme.

As a means of realizing selective S-modifications in NiSOD models, Harrop and co-workers developed a coordinatively unsaturated N_2S ligand that would allow for unconstrained modeling of a second S-ligand (S′) to complete the N_2SS′ coordination sphere.[43a] Reaction of the deprotonated form of the ligand nmp[2−] [dianion of N-(2-mercaptoethyl)-picolinamide] with Ni(II) ultimately led to an intractable S,S-bridged dimeric species, $[Ni_2(nmp)_2]$ (9). Complex 9 was initially thought to be an unusable precursor because of its poor solubility and the kinetic inertness of S,S-bridged square-planar Ni(II) complexes. However, reaction of 9 with different exogenous thiolates afforded the red-colored mononuclear square-planar Ni(II)−N_2S_2 species, $(Et_4N)[Ni(nmp)(SR)]$ (where R represents various alkyl and aromatic thiolate ligands), in very good yields (Figure 7). The nmp[2−] ligand
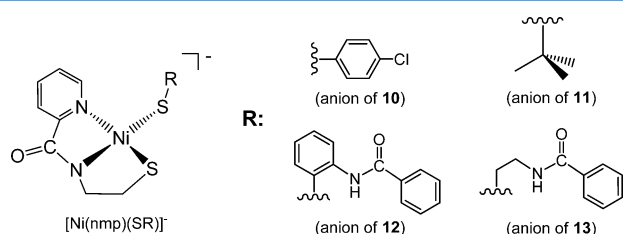

Figure 7. Structures of the NiSOD model complexes of the general formula $(Et_4N)[Ni(nmp)(SR)]$ [where R = C_6H_4-p-Cl in 10, ^tBu in 11, o-benzoylaminobenzene (o-babt) in 12, and N-(2-mercaptoethyl)-benzamide (meb) in 13]. The skewed line represents the point of attachment to the monodentate thiolate ligand.

replicates the two five-membered chelate rings formed by His1 and Cys2 in NiSOD, while the exogenous thiolate allows for unconstrained modeling of Cys6. Single-crystal X-ray analysis in combination with UV−vis, FTIR, ^{1}H NMR, CV, and ESI-MS of these complexes revealed a distorted planar coordination sphere with spectroscopic and electrochemical features similar to those of NiSOD$_{red}$. For example, the metric parameters for 10−13 [Ni−N_{amine}, 1.950 Å; Ni−$N_{carboxamide}$, 1.871 Å; Ni−$S_{trans-carboxamide}$, 2.193 Å; Ni−$S_{trans-amine}$, 2.155 Å (average values)][42a,b] are consistent with square-planar Ni(II)−N_2S_2 coordination (see 7 and 8). In complexes 10−13, the dominant electronic transition at ~450 nm masks the d−d bands due to the pyridine−N/Ni(II) CT (see Table 2). These complexes also displayed irreversible CVs consistent with ligand-based redox processes. Bulk oxidation studies revealed this to be the case with the oxidation occurring at the monodentate S-ligand to form disulfide and the insoluble S,S-bridged dimer 9. Regardless, the Ni−nmp constructs afforded suitable structural models of NiSOD$_{red}$ that could be modified at one specific coordination position.

To demonstrate the utility of this synthetic route, modifications such as appended H-bonding moieties were incorporated into the monodentate S-ligand [see complexes 10 and 12 (Figure 8)].[43b] These modifications are significant because NiSOD contains two key H-bonds to the coordinated cysteine thiolate trans to the peptide-N (Cys6).[14,29] The H-bonds in 12 and 13 were shown to be both intra- and intermolecular in nature. In both cases, the H-bond is bifurcated between both S-ligands in the basal plane, but more so with the monodentate thiolate (Figure 8). An
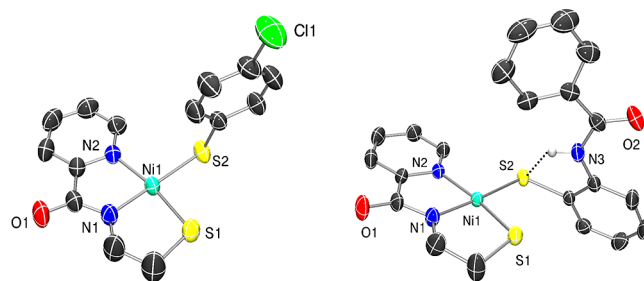

Figure 8. X-ray crystal structures of the anions of NiSOD$_{red}$ models $(Et_4N)[Ni(nmp)(SC_6H_4$-p-Cl)] (10, left) and $(Et_4N)[Ni(nmp)(S$-o-babt)] (12, right) highlighting intramolecular H-bonding between the carboxamide NH group (N3) and the monodentate thiolate (S2) in complex 12.

interesting feature is that H-bonding to sulfur resulted in a decrease in the Ni−S bond distance from the simple alkyl or aryl analogues (compare values of 2.2139 Å in 10 and 2.1939 Å in 12; 0.02 Å bond contraction). At first glance, this result is opposite to what one would predict on the basis of a decrease in the Lewis basicity of the H-bonded thiolate ligand. However, examination of the frontier MOs that govern this interaction in 10−13, as well as NiSOD$_{red}$, reveals that the HOMO is antibonding in nature with large and nearly equal contributions from both Ni-dπ AOs and S-pπ ligand orbitals, a so-called dπ−pπ repulsion (filled−filled interaction or four-electron repulsion). The Ni−S bond contraction in 12 and 13 is thus the result of stabilization of S-based ligand orbitals upon H-bonding, which results in a decrease in the filled−filled Ni dπ−S pπ antibonding interaction. Theoretical studies of truncated versions of NiSOD$_{red}$ reveal a similar contraction of 0.03 Å when the CysS ligands become fully protonated CysSH thiols.[18b] DFT calculations on 10−13 also show a decrease in the level of S-character in the HOMO (S-based MOs lower in energy) and an increase in the level of Ni-character upon incorporation of the H-bond to support more of a metal-based redox-active MO. The H-bonding interaction also resulted in an S-ligand that is less susceptible to reactions with electrophiles and/or oxidants such as O_2 with an overall stability gain of 15 kcal/mol at the S-atom with the H-bond. Thus, synthetically enforcing H-bond donors in these model complexes (also present at the NiSOD active site) decreases the nucleophilicity of a coordinated S-donor, stabilizes the Ni−S bond via relief of the dπ−pπ interaction, and serves as one potential mechanism that nature has incorporated to protect the CysS donors of NiSOD from oxidative modification and/or degradation during turnover.

Models 10−13 certainly afforded suitable structural analogues of NiSOD with variable synthetic manipulation at one S coordination position. The tunability of one S-ligand allowed this group to probe secondary-sphere interactions with coordinated S-ligands such as H-bonding, which proved to protect the sulfur from oxidation and promote more Ni-based redox. These models suffered, however, from a lack of water stability and solubility, thus limiting these studies to organic solvents. To achieve aqueous solubility and stability and ultimately superoxide chemistry, a new N_2S ligand utilizing a peptide backbone consisting of glycine and cysteine (denoted as GC-OMeH$_2$) was synthesized.[43c] Analogous to the previous Ni−nmp systems (10−13), reaction of GC-OMe[2−] with Ni(II) led to the expected S,S-bridged dimeric species $[Ni_2(GC-OMe)_2]$ (14) that was used in the construction of monomeric

Ni(II) complexes with variability at the fourth coordination position. Reaction of **14** with numerous exogenous thiolates afforded a variety of red/violet-colored mononuclear square-planar Ni(II)−N$_2$S$_2$ species of the general formula [Ni(GC-OMe)(SR)] (where R represents various alkyl and aromatic thiolate ligands) in good yields [**15−18** (Figure 9)]. EXAFS, in
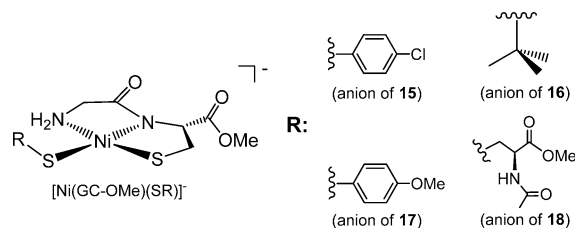

Figure 9. Structures of the NiSOD model complexes of the general formula K[Ni(GC-OMe)(SR)] (where R is C$_6$H$_4$-*p*-Cl in **15**, *t*Bu in **16**, C$_6$H$_4$-*p*-OMe in **17**, and *N*-acetyl-L-cysteine methyl ester or NAc in **18**). The skewed line represents the point of attachment to the monodentate thiolate ligand.

combination with UV−vis, FTIR, ^{1}H NMR, CV, and ESI-MS, of **15** and **17** revealed a distorted square-planar coordination (Ni−N$_{amine-avg}$, 1.99 Å; Ni−N$_{peptide-avg}$, 1.83 Å; Ni−S$_{avg}$, 2.17 Å) with spectroscopic and electrochemical features similar to those of NiSOD$_{red}$ and previous models [average λ_{max} = 480 nm (ε = 420 M^{-1} cm^{-1}) and 560 nm (ε = 200 M^{-1} cm^{-1}) in DMF] and an irreversible E_{ox} of ∼0.200 V (vs Ag/AgCl in DMF) (Table 2). Importantly, all of these measurements have been performed in organic solvents such as MeCN and a buffered (pH 7.4) aqueous medium, representing some of the first low-MW models to be probed under pseudophysiological conditions. These structurally characterized peptide-based Ni(II) complexes simulate many of the electronic features of NiSOD$_{red}$; however, they do not afford isolable Ni(III) species or superoxide-reactive systems, suggesting again the significance of the fifth His-N ligand in the enzyme. In fact, saturating solutions of these complexes with excess *N*-methylimidazole do not impart any electrochemical reversibility or other spectroscopic changes. Interestingly, the ^{1}H NMR spectra of **15−18** in D$_2$O or any protic solvent provide broad, ill-resolved signals that may correspond to variable solution speciation. It was hypothesized that these species could be solvent-bound or S-bridged oligomers because of the lability of the monodentate thiolate ligand. Addition of excess thiolate ligand afforded well-resolved spectra with a splitting pattern consistent with a

monomeric, diamagnetic square-planar Ni(II) complex. In contrast, dissolution of as-isolated **15−18** (from the synthesis) in aprotic solvents such as CD$_3$CN afforded neat, readily discernible ^{1}H NMR spectra consistent with one discrete species. These models suggest that the active site fragment of NiSOD may be rather dynamic with a propensity to oligomerize outside of the protein matrix (see the results from maquette system **3** described above). Thus, the surrounding environment and the N$_3$S$_2$ chelate may be crucial for maintaining coordinative integrity. In fact, mutagenesis of just one CysS to SerO (Cys6Ser or Cys2Ser) resulted in inactive enzyme with the addition of two new water ligands.[24] The absence of one cysteine thiolate promotes a high-spin (S = 1) aquated Ni(II) center at the NiSOD active site with no evidence of the remaining Ni−CysS bond in the mutants. This finding, coupled with the results for **15−18**, suggests more than redox-modulation and/or H$^+$-storage roles for cysteine in NiSOD. It is likely that the presence of both the Cys6 and Cys2 ligands in NiSOD is crucial for proper active site assembly and stabilization.

In an effort to obtain functional NiSOD complexes and to assess the role of the axial N-donor, Harrop's group designed and synthesized a 5C N$_3$S$_2$ ligand frame.[38] This ligand contained the appropriate donor atoms, in an electronic sense, that are situated in a spatial fashion exactly analogous to the active site of NiSOD. In fact, the presence of the axial N-donor ligand is hypothesized to stabilize, at least to some extent, the high-valent Ni(III) oxidation state (vide supra). If this hypothesis were correct, then an appropriately disposed Ni−N$_3$S$_2$ complex would be a significant step toward realizing catalytic function in NiSOD small molecule analogues and would explain the lack of reactivity of models **7−18**. The corresponding Ni(II) complex with this N$_3$S$_2$ ligand, namely K[Ni(N$_3$S$_2$)] [**19** (Figure 10)], was prepared by reacting the ligand with Ni(OAc)$_2$·4H$_2$O and NaOAc in MeOH to afford **19** in high yield.[41c] Complex **19** has been characterized by X-ray crystallography, UV−vis, FTIR, ^{1}H NMR, CV, and ESI-MS. Much like peptide models **15−18** described above, **19** also demonstrated excellent water solubility. Additionally, **19** is very stable in buffered media; no multiple speciation was observed as monitored by ^{1}H NMR and UV−vis spectroscopies. This stability is likely due to the chelate effect of the N$_3$S$_2$ ligand. The UV−vis spectrum of **19** in pH 7.5 PIPES buffer resembled the maquette and NiSOD$_{red}$ spectrum with double-humped ligand-field bands at 449 nm (ε = 230 M^{-1} cm^{-1}) and 570 nm (ε = 50 M^{-1} cm^{-1}) (Figure 10). The structural features are
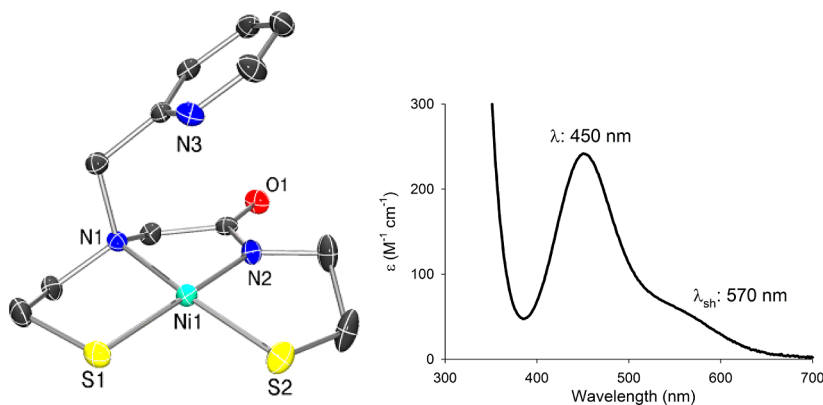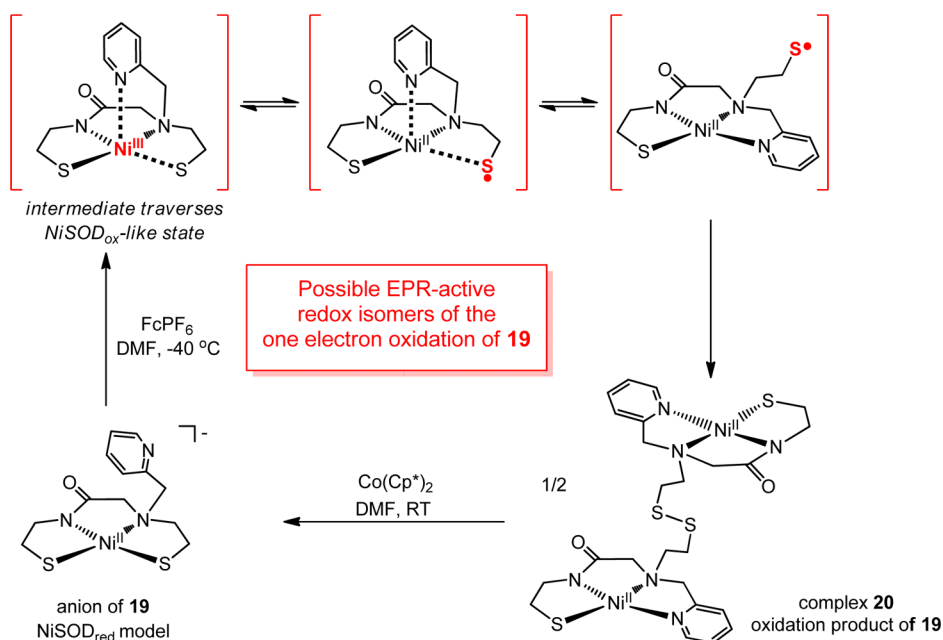

Figure 10. X-ray crystal structure of K[Ni(N$_3$S$_2$)] (**19**) (left) and electronic absorption spectrum of **19** in pH 7.5 PIPES buffer at 25 °C (right).

Scheme 1. Proposed Mechanism of the Oxidative Conversion of NiSOD_red Model Complex 19 to Disulfide-Linked Complex 20[a]

[a]Hypothesized intermediates are shown in red brackets, with paramagnetic atoms shown in bold and colored red. $FcPF_6$ is the chemical oxidant ferrocenium hexafluorophosphate; $Co(Cp^*)_2$ is the chemical reductant decamethylcobaltocene. This scheme was adapted from ref 41c.

comparable to prior models (see Table 2) featuring a 4C Ni(II)−N_2S_2 planar complex with the only exception of the noncoordinated pyridine-N situated ∼3.2 Å and tilted away from the metal. The Ni−N_{py} distance of this potential fifth ligand and the tilt of the pyridine plane are structurally analogous to the values observed for NiSOD_red. The electrochemistry of **19** displayed the typical irreversible behavior even with a potential N-donor in the ligand frame with an E_{ox} of −0.125 V (DMF vs Ag/AgCl). However, a new reduction wave was found at E_{red} = −1.44 V, which only appeared when the oxidized species was traversed. The large ΔE_p (∼1.2 V) suggested that a significant structural rearrangement occurred during the redox process. To identify the site of the redox process, bulk oxidation was performed with Fc^+, which resulted in dinuclear disulfide-linked species **20** that formed from a transient 5C Ni(III) intermediate (Scheme 1). Interestingly, the S atoms in the disulfide linkage of **20** originate from the S-donor *trans* to the carboxamide-N in **19**, highlighting the lability of this particular ligand and potentially Cys6 in NiSOD. This conversion mimics the same redox and coordination geometry change as observed in NiSOD. While the results suggested that the axial His1-Im ligand in NiSOD is not entirely responsible for Ni-based redox, it still appears to be critical for keeping the coordination sphere intact to prevent polymeric RSSR formation. Thus, His1-N binding in combination with the protein structure is primarily responsible for Ni(III/II) cycling in NiSOD. Further support for this hypothesis comes from theoretical studies of the enzyme, which suggest a primarily S-based HOMO in NiSOD_red[18b] along with the long Ni(III)−$N_{imidazole}$ distance (∼2.5 Å) observed in NiSOD_ox.[14]

■ SUMMARY AND OUTLOOK

NiSOD presents numerous structural and spectroscopic characteristics that distinguish it from other members of the SOD family; however, it is certainly representative of redox-active Ni metalloenzymes. As such, the results of synthetic modeling work have revealed valuable information regarding the properties of this unique Ni coordination environment. It is evident that the mixed amine/peptide-N ligands assist in the stabilization of high-valent Ni(III) as well as the low-spin electronic configuration of the metal. It is believed that the unique asymmetric N-donor set, in combination with the two CysS-donors, sufficiently depresses the Ni(III/II) redox couple so that it is physiologically accessible and within the window of the superoxide redox potentials. All of the models report redox potentials in this range (see Tables 1 and 2). The $N_{amine}N_{carboxamide}S_2$ coordination environment also provides kinetic stability against O_2 and H_2O_2 (the products of SOD) under turnover conditions as noted in several analogues. Some of the model systems demonstrate SOD functionality albeit at rates significantly lower than that of the enzyme. Of these functional models, most contain an axial N-ligand. Indeed, NiSOD His1 mutants and certain maquette models that do not have this ligand demonstrate low activity. We suspect that this ligand is crucial in NiSOD. While approximate models such as **5** highlight the potential for functionality even in the absence of a fifth ligand, it appears that the basic requisite for SOD activity is a low-spin Ni center with the correct redox potential (see complex **6** that contains biologically irrelevant alkoxy ligands). To underscore the importance of His1 in terms of NiSOD function, the Ni(III) state is only achieved, at least transiently, in low-MW accurate models that contain this or a similar type of ligand (e.g., py-N).

With regard to the NiSOD catalytic mechanism, the synthetic analogue, biochemical, and theoretical data have led to the following postulates. The 4C square-planar NiSOD_red site observed in the crystal structure is likely a resting state of the enzyme that is not catalytically active. Indeed, models such as **7−18** that accurately reproduce the structure and electronic spectrum of NiSOD_red but lack a fifth axial N-ligand exhibit mostly irreversible redox potentials (ligand-based redox

processes, disulfide formation) and no SOD activity. The one system that displays quasi-reversible redox behavior (**7**) has never been isolated or proven to be Ni(III). This result can be explained by the electronic structure that defines the nature of the frontier MO involved in this redox process. This MO has significant contributions of both S-pπ and Ni-dπ character, which are symptomatic of a highly covalent Ni−S bond (Figure 11). In theoretical studies of NiSOD, this MO exhibits
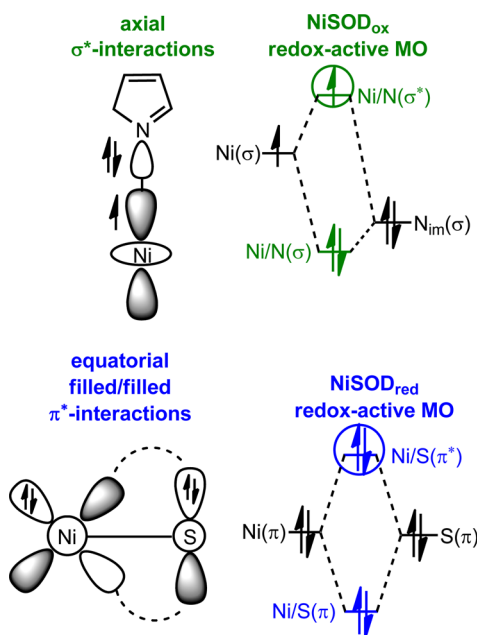

Figure 11. Frontier MOs and illustration of the dominant bonding interactions in NiSOD$_{ox}$ (top) and NiSOD$_{red}$ (bottom). This figure was adapted from ref 18b.

predominantly S-pπ character as well (HOMO, 26% Ni-dπ and 66% S-pπ; HOMO-1, 36% Ni-dπ and 45% S-pπ).[18b] This result is not at all unique to NiSOD$_{red}$ and has been demonstrated in all accurate Ni(II)−N$_2$S$_2$ models (**7−19**), which display significant contributions from both Ni and S in this redox-active MO. This begs the question of what prevents S-oxidation in the enzyme. One possibility is that NiSOD has evolved to prevent S-oxidation by destabilizing the Ni-based AOs or by stabilizing the S-based ligand group orbitals by some mechanism that cannot be modeled accurately by DFT. Either change will yield a redox-active MO with more Ni-character. Stabilization of S-based orbitals has been demonstrated through H-bonding interactions both computationally[30a,b,33a] and experimentally[43b] to increase the level of Ni character and decrease the nucleophilicity (viz. oxygen reactivity) of the H-bonded sulfur. In addition to S-protection from ROS, full protonation of the coordinated cysteinates to cysteine thiols could serve as a reservoir for H$^+$ in the formation of H$_2$O$_2$ (eq 2). This proposal has been advocated by separate DFT studies.[30b,33a] Another postulate is that the Ni center remains 5C throughout catalysis.[30b,39b] Examination of the electronic structure of NiSOD$_{ox}$ reveals a redox-active MO with predominantly Ni-dσ character that is antibonding with respect to the Ni-d$_{z^2}$(dσ) AO and N-pσ orbital of the axial His ligand (Figure 11).[18b] This electronic structure explains the hyperfine feature in the EPR as well as the relatively long Ni−HisN bond in the NiSOD structures. If this orbital was the redox-active MO during catalysis, then one would expect the Ni−HisN

distance to vary during turnover, which would result in the atypical Ni−Im distance. This analysis excludes the effects imparted by the H-bonding network, His1-Glu17-Arg47. A 5C active species would also minimize the reorganizational energy (λ) that occurs during eT, which has been suggested for functional maquette system **2**.[39b] This explanation makes intuitive sense as eT rates are inherently faster than bond-forming and/or -breaking rates. Additionally, all model systems that have been isolated in the Ni(III) form contain the Im axial ligand. We thus propose the mechanism as highlighted in Scheme 2. The debate over outer-sphere versus inner-sphere

Scheme 2. Proposed Active Forms of NiSOD during Outer-Sphere Turnover (black) and Potential Inner-Sphere Intermediates (gray, I and II)[a]
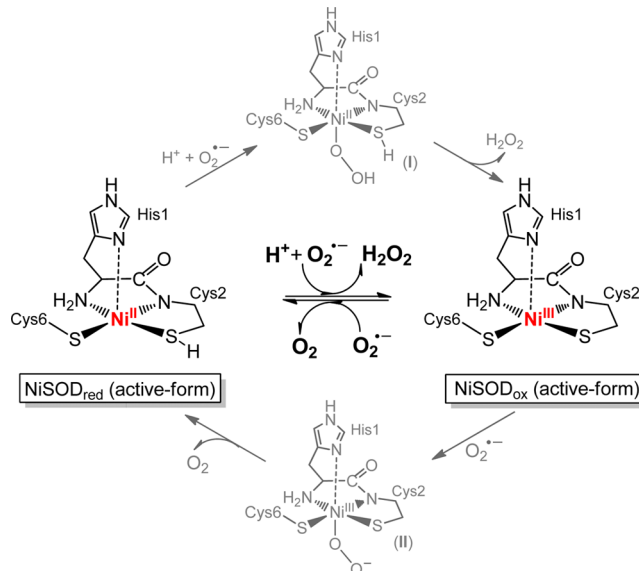
[a]Intermediate I may also be viewed as a Ni(III)−hydroperoxo species after internal transfer of an electron from Ni(II) to the coordinated hydrosuperoxo. The dashed line from HisN to Ni implies a relatively long bond as observed in the X-ray crystal structures of NiSOD (see refs 14 and 15). The protonation of both cysteinates has not been widely established; however, either cysteine is a likely candidate, and we have chosen Cys2 in this depiction for the sake of clarity. If only one CysSH is present, a protonated hydrosuperoxo radical (HOO$^{\bullet}$) has been proposed to enter the active site (see ref 30b) despite the known superoxide pK_a of 4.8.

redox still remains, and we will not attempt to elect one in the present account, although their differences are noted in Scheme 2. Most of the biochemical evidence points toward an outer-sphere mechanism that includes (i) the lack of rate dependence on the ionic strength of the medium, (ii) no evidence of small anions such as N$_3^-$, even in large excess, binding to Ni, and (iii) the presence of a noncoordinated Cl$^-$ ligand in the X-ray structure of the NiSOD Tyr9Phe mutant positioned ∼3.5 Å from the Ni center (a suggested superoxide binding site). An outer-sphere mechanism would also keep ROS away from and protect the CysS-ligands from S-oxidation and/or oxygenation. To date, most of the model work is supportive of this proposal. However, evidence of CN$^-$ binding in some maquette models and theoretical studies of substrate coordination suggest otherwise. We anticipate that the bioinorganic synthetic modeling community will have a significant role in addressing these outlying issues in future NiSOD analogue systems.

■ AUTHOR INFORMATION

Corresponding Author

*Phone: (706) 542-3486. Fax: (706) 542-9454. E-mail: tharrop@uga.edu.

Author Contributions

The manuscript was written through contributions of all authors. All authors have given approval to the final version of the manuscript.

Author Contributions

E.P.B. and P.T.T. contributed equally to this work.

■ REFERENCES

(1) Valentine, J. S., Wertz, D. L., Lyons, T. J., Liou, L.-L., Goto, J. J., and Gralla, E. B. (1998) The dark side of dioxygen biochemistry. *Curr. Opin. Chem. Biol. 2*, 253–262.

(2) McCord, J. M. (2003) Oxidative stress related diseases—overview. In *Critical Reviews of Oxidative Stress and Aging: Advances in Basic Science, Diagnostics, and Intervention* (Rodriguez, H., and Cutler, R., Eds.) pp 883–895, World Scientific Publishing, Singapore.

(3) Maritim, A. C., Sanders, R. A., and Watkins, J. B., III (2003) Diabetes, Oxidative Stress, and Antioxidants: A Review. *J. Biochem. Mol. Toxicol. 17*, 24–38.

(4) Kocatürk, P. A., Akbostanci, M. C., Tan, F., and Kavas, G. Ö. (2000) Superoxide dismutase activity and zinc and copper concentrations in Parkinson's disease. *Pathophysiology 7*, 63–67.

(5) De Leo, M. E., Borrello, S., Passantino, M., Palazzotti, B., Mordente, A., Daniele, A., Filippini, V., Galeotti, T., and Masullo, C. (1998) Oxidative stress and overexpression of manganese superoxide dismutase in patients with Alzheimer's disease. *Neurosci. Lett. 250*, 173–176.

(6) Fortunato, G., Pastinese, A., Intrieri, M., Lofrano, M. M., Gaeta, G., Censi, M. B., Boccalatte, A., Salvatore, F., and Sacchetti, L. (1997) Serum Mn-Superoxide Dismutase in Acute Myocardial Infarction. *Clin. Biochem. 30*, 569–571.

(7) (a) Miller, A.-F. (2004) Superoxide dismutases: Active sites that save, but a protein that kills. *Curr. Opin. Chem. Biol. 8*, 162–168. (b) Fridovich, I. (2004) Superoxide Dismutase. In *Encyclopedia of Biological Chemistry* (Lennarz, W. J., and Lane, M. D., Eds.) 1st ed., Vol. 4, pp 135–138, Elsevier, New York.

(8) Tainer, J. A., Getzoff, E. D., Richardson, J. S., and Richardson, D. C. (1983) Structure and mechanism of copper, zinc superoxide dismutase. *Nature 306*, 284–287.

(9) (a) Borgstahl, G. E. O., Parge, H. E., Hickey, M. J., Beyer, W. F., Jr., Hallewell, R. A., and Tainer, J. A. (1992) The structure of human mitochondrial manganese superoxide dismutase reveals a novel tetrameric interface of two 4-helix bundles. *Cell 71*, 107–118.

(b) Grove, L. E., and Brunold, T. C. (2008) Second-Sphere Tuning of the Metal Ion Reduction Potentials in Iron and Manganese Superoxide Dismutases. *Comments Inorg. Chem. 29*, 134–168. (c) Miller, A.-F. (2008) Redox Tuning over Almost 1 V in a Structurally Conserved Active Site: Lessons from Fe-Containing Superoxide Dismutase. *Acc. Chem. Res. 41*, 501–510.

(10) (a) Tierney, D. L., Fee, J. A., Ludwig, M. L., and Penner-Hahn, J. E. (1995) X-ray Absorption Spectroscopy of the Iron Site in *Escherichia coli* Fe(III) Superoxide Dismutase. *Biochemistry 34*, 1661–1668. (b) Grove, L. E., Xie, J., Yikilmaz, E., Karapetyan, A., Miller, A.-F., and Brunold, T. C. (2008) Spectroscopic and Computational Insights into Second-Sphere Amino-Acid Tuning of Substrate Analogue/Active-Site Interactions in Iron(III) Superoxide Dismutase. *Inorg. Chem. 47*, 3993–4004.

(11) Brown, R. H., Jr. (1998) SOD1 aggregates in ALS: Cause, correlate or consequence? *Nat. Med. 4*, 1362–1364.

(12) Youn, H.-D., Youn, H., Lee, J.-W., Yim, Y.-I., Lee, J. K., Hah, Y. C., and Kang, S.-O. (1996) Unique Isozymes of Superoxide Dismutase in *Streptomyces griseus. Arch. Biochem. Biophys. 334*, 341–348.

(13) Palenik, B., Brahamsha, B., Larimer, F. W., Land, M., Hauser, L., Chain, P., Lamerdin, J., Regala, W., Allen, E. E., McCarren, J., Paulsen, I., Dufresne, A., Partensky, F., Webb, E. A., and Waterbury, J. (2003) The genome of a motile marine *Synechococcus. Nature 424*, 1037–1042.

(14) Barondeau, D. P., Kassmann, C. J., Bruns, C. K., Tainer, J. A., and Getzoff, E. D. (2004) Nickel Superoxide Dismutase Structure and Mechanism. *Biochemistry 43*, 8038–8047.

(15) Wuerges, J., Lee, J.-W., Yim, Y.-I., Yim, H.-S., Kang, S.-O., and Carugo, K. D. (2004) Crystal structure of nickel-containing superoxide dismutase reveals another type of active site. *Proc. Natl. Acad. Sci. U.S.A. 101*, 8569–8574.

(16) Herbst, R. W., Guce, A., Bryngelson, P. A., Higgins, K. A., Ryan, K. C., Cabelli, D. E., Garman, S. C., and Maroney, M. J. (2009) Role of Conserved Tyrosine Residues in NiSOD Catalysis: A Case of Convergent Evolution. *Biochemistry 48*, 3354–3369.

(17) Harrop, T. C., and Mascharak, P. K. (2006) Model Complexes of Ni-Containing Enzymes. In *Concepts and Models in Bioinorganic Chemistry* (Kraatz, H.-B., and Metzler-Nolte, N., Eds.) pp 309–329, Wiley-VCH, Weinheim, Germany.

(18) (a) Choudhury, S. B., Lee, J.-W., Davidson, G., Yim, Y.-I., Bose, K., Sharma, M. L., Kang, S.-O., Cabelli, D. E., and Maroney, M. J. (1999) Examination of the Nickel Site Structure and Reaction Mechanism in *Streptomyces seoulensis* Superoxide Dismutase. *Biochemistry 38*, 3744–3752. (b) Fiedler, A. T., Bryngelson, P. A., Maroney, M. J., and Brunold, T. C. (2005) Spectroscopic and Computational Studies of Ni Superoxide Dismutase: Electronic Structure Contributions to Enzymatic Function. *J. Am. Chem. Soc. 127*, 5449–5462.

(19) Krüger, H.-J., Peng, G., and Holm, R. H. (1991) Low-Potential Nickel(III,II) Complexes: New Systems Based on Tetradentate Amidate-Thiolate Ligands and the Influence of Ligand Structure on Potentials in Relation to the Nickel Site in [NiFe]-Hydrogenases. *Inorg. Chem. 30*, 734–742.

(20) Fiedler, A. T., and Brunold, T. C. (2007) Spectroscopic and Computational Studies of Ni^{3+} Complexes with Mixed S/N Ligation: Implications for the Active Site of Nickel Superoxide Dismutase. *Inorg. Chem. 46*, 8511–8523.

(21) (a) Xiao, Y., Wang, H., George, S. J., Smith, M. C., Adams, M. W. W., Jenney, F. E., Jr., Sturhahn, W., Alp, E. E., Zhao, J., Yoda, Y., Dey, A., Solomon, E. I., and Cramer, S. P. (2005) Normal Mode Analysis of *Pyrococcus furiosus* Rubredoxin via Nuclear Resonance Vibrational Spectroscopy (NRVS) and Resonance Raman Spectroscopy. *J. Am. Chem. Soc. 127*, 14596–14606. (b) Han, S., Czernuszewicz, R. S., Kimura, T., Adams, M. W. W., and Spiro, T. G. (1989) Fe_2S_2 Protein Resonance Raman Spectra Revisited: Structural Variations among Adrenodoxin, Ferredoxin, and Red Paramagnetic Protein. *J. Am. Chem. Soc. 111*, 3505–3511.

(22) (a) Qiu, D., Kilpatrick, L., Kitajima, N., and Spiro, T. G. (1994) Modeling Blue Copper Protein Resonance Raman Spectra with

Thiolate-Cu^{II} Complexes of a Sterically Hindered Tris(pyrazolyl)-borate. *J. Am. Chem. Soc. 116*, 2585−2590. (b) Qiu, D., Dasgupta, S., Kozlowski, P. M., Goddard, W. A., III, and Spiro, T. G. (1998) Chromophore-in-Protein Modeling of the Structures and Resonance Raman Spectra for Type 1 Copper Proteins. *J. Am. Chem. Soc. 120*, 12791−12797.

(23) Bryngelson, P. A., Arobo, S. E., Pinkham, J. L., Cabelli, D. E., and Maroney, M. J. (2004) Expression, Reconstitution, and Mutation of Recombinant *Streptomyces coelicolor* NiSOD. *J. Am. Chem. Soc. 126*, 460−461.

(24) (a) Ryan, K. C., Johnson, O. E., Cabelli, D. E., Brunold, T. C., and Maroney, M. J. (2010) Nickel superoxide dismutase: Structural and functional roles of Cys2 and Cys6. *J. Biol. Inorg. Chem. 15*, 795−807. (b) Johnson, O. E., Ryan, K. C., Maroney, M. J., and Brunold, T. C. (2010) Spectroscopic and computational investigation of three Cys-to-Ser mutants of nickel superoxide dismutase: Insight into the roles played by the Cys2 and Cys6 active-site residues. *J. Biol. Inorg. Chem. 15*, 777−793.

(25) (a) Lawrence, G. D., and Sawyer, D. T. (1979) Potentiometric Titrations and Oxidation-Reduction Potentials of Manganese and Copper-Zinc Superoxide Dismutases. *Biochemistry 18*, 3045−3050. (b) Barrette, W. C., Jr., Sawyer, D. T., Fee, J. A., and Asada, K. (1983) Potentiometric Titrations and Oxidation-Reduction Potentials of Several Iron Superoxide Dismutases. *Biochemistry 22*, 624−627.

(26) Sawyer, D. T., and Valentine, J. S. (1981) How Super is Superoxide? *Acc. Chem. Res. 14*, 393−400.

(27) Uudsemaa, M., and Tamm, T. (2003) Density-Functional Theory Calculations of Aqueous Redox Potentials of Fourth-Period Transition Metals. *J. Phys. Chem. A 107*, 9997−10003.

(28) Shearer, J., Dehestani, A., and Abanda, F. (2008) Probing Variable Amine/Amide Ligation in Ni^{II}N$_2$S$_2$ Complexes Using Sulfur K-Edge and Nickel L-Edge X-ray Absorption Spectroscopies: Implications for the Active Site of Nickel Superoxide Dismutase. *Inorg. Chem. 47*, 2649−2660.

(29) Grapperhaus, C. A., and Darensbourg, M. Y. (1998) Oxygen Capture by Sulfur in Nickel Thiolates. *Acc. Chem. Res. 31*, 451−459.

(30) (a) Mullins, C. S., Grapperhaus, C. A., and Kozlowski, P. M. (2006) Density functional theory investigations of NiN$_2$S$_2$ reactivity as a function of nitrogen donor type and N−H···S hydrogen bonding inspired by nickel-containing superoxide dismutase. *J. Biol. Inorg. Chem. 11*, 617−625. (b) Pelmenschikov, V., and Siegbahn, P. E. M. (2006) Nickel Superoxide Dismutase Reaction Mechanism Studied by Hybrid Density Functional Methods. *J. Am. Chem. Soc. 128*, 7466−7475. (c) Neupane, K. P., and Shearer, J. (2006) The Influence of Amine/Amide versus Bisamide Coordination in Nickel Superoxide Dismutase. *Inorg. Chem. 45*, 10552−10566.

(31) (a) Zilbermann, I, Maimon, E., Cohen, H., and Meyerstein, D. (2005) Redox Chemistry of Nickel Complexes in Aqueous Solutions. *Chem. Rev. 105*, 2609−2625. (b) Halcrow, M. A., and Christou, G. (1994) Biomimetic Chemistry of Nickel. *Chem. Rev. 94*, 2421−2481.

(32) (a) Ragsdale, S. W. (1998) Nickel Biochemistry. *Curr. Opin. Chem. Biol. 2*, 208−215. (b) Ragsdale, S. W. (2009) Nickel-based Enzyme Systems. *J. Biol. Chem. 284*, 18571−18575.

(33) (a) Prabhakar, R., Morokuma, K., and Musaev, D. G. (2006) A DFT Study of the Mechanism of Ni Superoxide Dismutase (NiSOD): Role of the Active Site Cysteine-6 Residue in the Oxidative Half-Reaction. *J. Comput. Chem. 27*, 1438−1445. (b) Szilagyi, R. K., Bryngelson, P. A., Maroney, M. J., Hedman, B., Hodgson, K. O., and Solomon, E. I. (2004) S K-Edge X-ray Absorption Spectroscopic Investigation of the Ni-Containing Superoxide Dismutase Active Site: New Structural Insight into the Mechanism. *J. Am. Chem. Soc. 126*, 3018−3019.

(34) Lanzilotta, W. N., Schuller, D. J., Thorsteinsson, M. V., Kerby, R. L., Roberts, G. P., and Poulos, T. L. (2000) Structure of the CO sensing transcription activator CooA. *Nat. Struct. Mol. Biol. 7*, 876−880.

(35) Nagashima, S., Nakasako, M., Dohmae, N., Tsujimura, M., Takio, K., Odaka, M., Yohda, M., Kamiya, N., and Endo, I. (1998) Novel non-heme iron center of nitrile hydratase with a claw setting of oxygen atoms. *Nat. Struct. Mol. Biol. 5*, 347−351.

(36) Darnault, C., Volbeda, A., Kim, E. J., Legrand, P., Vernède, X., Lindahl, P. A., and Fontecilla-Camps, J. C. (2003) Ni-Zn-[Fe$_4$-S$_4$] and Ni-Ni-[Fe$_4$-S$_4$] clusters in closed and open α subunits of acetyl-CoA synthase/carbon monoxide dehydrogenase. *Nat. Struct. Mol. Biol. 10*, 271−279.

(37) Peters, J. W., Stowell, M. H. B., Soltis, S. M., Finnegan, M. G., Johnson, M. K., and Rees, D. C. (1997) Redox-Dependent Structural Changes in the Nitrogenase P-Cluster. *Biochemistry 36*, 1181−1187.

(38) Ibers, J. A., and Holm, R. H. (1980) Modeling Coordination Sites in Metallobiomolecules. *Science 209*, 223−235.

(39) (a) Shearer, J., and Long, L. M. (2006) A Nickel Superoxide Dismutase Maquette That Reproduces the Spectroscopic and Functional Properties of the Metalloenzyme. *Inorg. Chem. 45*, 2358−2360. (b) Neupane, K. P., Gearty, K., Francis, A., and Shearer, J. (2007) Probing Variable Axial Ligation in Nickel Superoxide Dismutase Utilizing Metallopeptide-Based Models: Insight into the Superoxide Disproportionation Mechanism. *J. Am. Chem. Soc. 129*, 14605−14618. (c) Shearer, J., Neupane, K. P., and Callan, P. E. (2009) Metallopeptide Based Mimics with Substituted Histidines Approximate a Key Hydrogen Bonding Network in the Metalloenzyme Nickel Superoxide Dismutase. *Inorg. Chem. 48*, 10560−10571. (d) Schmidt, M., Zahn, S., Carella, M., Ohlenschläger, O., Görlach, M., Kothe, E., and Weston, J. (2008) Solution Structure of a Functional Biomimetic and Mechanistic Implications for Nickel Superoxide Dismutases. *ChemBioChem 9*, 2135−2146. (e) Tietze, D., Breitzke, H., Imhof, D., Kothe, E., Weston, J., and Buntkowsky, G. (2009) New Insight into the Mode of Action of Nickel Superoxide Dismutase by Investigating Metallopeptide Substrate Models. *Chem.—Eur. J. 15*, 517−523. (f) Tietze, D., Tischler, M., Voigt, S., Imhof, D., Ohlenschläger, O., Görlach, M., and Buntkowsky, G. (2010) Development of a Functional *cis*-Prolyl Bond Biomimetic and Mechanistic Implications for Nickel Superoxide Dismutase. *Chem.—Eur. J. 16*, 7572−7578. (g) Tietze, D., Voigt, S., Mollenhauer, D., Tischler, M., Imhof, D., Gutmann, T., González, L., Ohlenschläger, O., Breitzke, H., Görlach, M., and Buntkowsky, G. (2011) Revealing the Position of the Substrate in Nickel Superoxide Dismutase: A Model Study. *Angew. Chem., Int. Ed. 50*, 2946−2950. (h) Krause, M. E., Glass, A. M., Jackson, T. A., and Laurence, J. S. (2010) Novel Tripeptide Model of Nickel Superoxide Dismutase. *Inorg. Chem. 49*, 362−364. (i) Krause, M. E., Glass, A. M., Jackson, T. A., and Laurence, J. S. (2011) MAPping the Chiral Inversion and Structural Transformation of a Metal-Tripeptide Complex Having Ni-Superoxide Dismutase Activity. *Inorg. Chem. 50*, 2479−2487. (j) Glass, A. M., Krause, M. E., Laurence, J. S., and Jackson, T. A. (2012) Controlling the Chiral Inversion Reaction of the Metallopeptide Ni-Asparagine-Cysteine-Cysteine with Dioxygen. *Inorg. Chem. 51*, 10055−10063.

(40) (a) Ma, H., Chattopadhyay, S., Petersen, J. L., and Jensen, M. P. (2008) Harnessing Scorpionate Ligand Equilibria for Modeling Reduced Nickel Superoxide Dismutase Intermediates. *Inorg. Chem. 47*, 7966−7968. (b) Ma, H., Wang, G., Yee, G. T., Petersen, J. L., and Jensen, M. P. (2009) Scorpionate-supported models of nickel-dependent superoxide dismutase. *Inorg. Chim. Acta 362*, 4563−4569. (c) Lee, W.-Z., Chiang, C.-W., Lin, T.-H., and Kuo, T.-S. (2012) A Discrete Five-Coordinate Ni^{III} Complex Resembling the Active Site of the Oxidized Form of Nickel Superoxide Dismutase. *Chem.—Eur. J. 18*, 50−53. (d) Nakane, D., Funahashi, Y., Ozawa, T., and Masuda, H. (2010) A Square-planar Ni(II) Complex with an Asymmetric N$_2$S$_2$ Donor Set as a Model for the Active Site of Nickel-containing SOD: Structural Conversion Driven by Addition of a Strong Donor Ligand in the High Oxidation State. *Chem. Lett. 39*, 344−346.

(41) (a) Shearer, J., and Zhao, N. (2006) [Me$_4$N](Ni^{II}(BEAAM)): A Synthetic Model for Nickel Superoxide Dismutase That Contains Ni in a Mixed Amine/Amide Coordination Environment. *Inorg. Chem. 45*, 9637−9639. (b) Mathrubootham, V., Thomas, J., Staples, R., McCraken, J., Shearer, J., and Hegg, E. L. (2010) Bisamidate and Mixed Amine/Amidate NiN$_2$S$_2$ Complexes as Models for Nickel-Containing Acetyl Coenzyme A Synthase and Superoxide Dismutase:

An Experimental and Computational Study. *Inorg. Chem.* 49, 5393–5406. (c) Gale, E. M., Simmonett, A. C., Telser, J., Schaefer, H. F., III, and Harrop, T. C. (2011) Toward Functional Ni-SOD Biomimetics: Achieving a Structural/Electronic Correlation with Redox Dynamics. *Inorg. Chem.* 50, 9216–9218.

(42) (a) Jenkins, R. M., Singleton, M. L., Almaraz, E., Reibenspies, J. H., and Darensbourg, M. Y. (2009) Imidazole-Containing (N_3S)-Ni^{II} Complexes Relating to Nickel Containing Biomolecules. *Inorg. Chem.* 48, 7280–7293. (b) Mullins, C. S., Grapperhaus, C. A., Frye, B. C., Wood, L. H., Hay, A. J., Buchanan, R. M., and Mashuta, M. S. (2009) Synthesis and Sulfur Oxygenation of a (N_3S)Ni Complex Related to Nickel-Containing Superoxide Dismutase. *Inorg. Chem.* 48, 9974–9976. (c) Herdt, D. R., and Grapperhaus, C. A. (2012) Kinetic study of nickel-thiolate oxygenation by hydrogen peroxide. Implications for nickel-containing superoxide dismutase. *Dalton Trans.* 41, 364–366.

(43) (a) Gale, E. M., Patra, A. K., and Harrop, T. C. (2009) Versatile Methodology Toward NiN_2S_2 Complexes as Nickel Superoxide Dismutase Models: Structure and Proton Affinity. *Inorg. Chem.* 48, 5620–5622. (b) Gale, E. M., Narendrapurapu, B. S., Simmonett, A. C., Schaefer, H. F., III, and Harrop, T. C. (2010) Exploring the Effects of H-Bonding in Synthetic Analogues of Nickel Superoxide Dismutase (Ni-SOD): Experimental and Theoretical Implications for Protection of the Ni–SCys Bond. *Inorg. Chem.* 49, 7080–7096. (c) Gale, E. M., Cowart, D. M., Scott, R. A., and Harrop, T. C. (2011) Dipeptide-Based Models of Nickel Superoxide Dismutase: Solvent Effects Highlight a Critical Role to Ni–S Bonding and Active Site Stabilization. *Inorg. Chem.* 50, 10460–10471.

(44) Colpas, G. J., Maroney, M. J., Bagyinka, C., Kumar, M., Willis, W. S., Suib, S. L., Baidya, N., and Mascharak, P. K. (1991) X-ray Spectroscopic Studies of Nickel Complexes, with Application to the Structure of Nickel Sites in Hydrogenases. *Inorg. Chem.* 30, 920–928.

(45) Hanss, J., and Krüger, H.-J. (1998) First Isolation and Structural Characterization of a Nickel(III) Complex Containing Aliphatic Thiolate Donors. *Angew. Chem., Int. Ed.* 37, 360–363.

(46) (a) Connelly, N. G., and Geiger, W. E. (1996) Chemical Redox Agents for Organometallic Chemistry. *Chem. Rev.* 96, 877–910. (b) Bard, A. J., and Faulkner, L. R. (2000) *Electrochemical Methods: Fundamentals and Applications*, 2nd ed., John Wiley and Sons, New York.